Chapter 8

Supported Nickel-Based Catalysts for Partial Hydrogenation of Edible Oils

Miroslav Stanković, Jugoslav Krstić, Margarita Gabrovska, Vojkan Radonjić, Dimitrinka Nikolova, Davor Lončarević and Dušan Jovanović

Additional information is available at the end of the chapter

http://dx.doi.org/10.5772/66967

Abstract

Nickel-based catalysts, supported on diatomite, silica gel and perlite, with high nickel loadings, have been prepared by precipitation-deposition method. Various nickel precursor salts were used for the preparation of catalyst precursors. In the precursor state, the catalysts were characterized using nitrogen physisorption, mercury porosimetry, infrared, and X-ray diffraction spectroscopy. The reducibility of catalyst precursors was evaluated using hydrogen temperature programmed reduction. Hydrogen chemisorption and X-ray photoelectron spectroscopy measurements were performed with the aim of characterizing the chemical state of the catalyst precursors. This research was focused on the study of some major factors on the state, dispersion and reducibility of a deposited Ni^{2+} phase by the combined use of mentioned experimental techniques. We have examined the influence of the nature of support and the use of modifiers on activity of nickel-based catalysts in the partial hydrogenation of sunflower and soybean oils. Nitrogen physisorption and mercury porosimetry data showed that synthesis operating conditions and pore structure of supports have a profound effect on the textural properties of catalyst precursors. The analysis of infrared and X-ray diffraction spectra showed the existence of chemical species and phases which indicate the different extent of interaction between the support and the active metal. Temperature programmed reduction study revealed that the reduction features depend on the identity of the nickel precursor salt and its interaction with the support. A stronger interaction of the supported Ni^{2+} phase with support hinders the reduction of catalyst precursors. Hydrogen chemisorption results showed the presence of nickel crystallites varying from 5 to 47 nm in size. The X-ray photoelectron spectroscopy data confirmed the formation surface species with different strength of interaction and different nickel crystallite sizes. The hydrogenation results showed significant differences, depending on the support and the modifier, as well as structural characteristics of reduced catalyst precursors. The results show the importance of modifiers in the control of the activity and selectivity of the partial hydrogenation

process. The developed kinetic models of the hydrogenation of soybean and sunflower oils over studied catalytic systems were found useful in the prediction of the rate of reactions, product selectivity and catalytic activity.

Keywords: hydrogenation, soybean oil, sunflower oil, *trans* fatty acids, nickel catalysts, diatomite, silica gel, perlite, activity, selectivity, kinetics

1. Introduction

Hydrogenation of edible oils is a process used since its development in the early 1900s, to convert ats [1]. Principal products obtained by hydrogenation include oleomargarine stock, shortening, salad and cooking oils [2]. Hydrogenation changes the melting and solidification characteristics of the oils and is usually employed to reduce the degree of unsaturation of the naturally occurring triacylglycerides (TAGs). Most of the unsaturated fatty acids in TAGs contain 18 carbon atoms and the unsaturated fatty acids are almost completely in *cis*-configuration. The degree of hydrogenation which leads to hardening of the oil depends on the application, but it is always desired to reduce the level of polyunsaturated fatty acids such as linolenic (C18:3) and linoleic (C18:2) acids due to their high sensitivity to oxidation [3, 4]. This process is commonly used for vegetable oils with significant levels of linoleic acid, such as soybean and sunflower oils [5].

The hydrogenation process is usually carried out in a three-phase slurry reactor in a semi-batch mode where hydrogen gas is bubbled with pressure in hot vegetable oil in the presence of a catalyst [6]. In the industrial practice, hydrogenation process is typically carried out using nickel-based catalysts, either in the form of nickels Raney, or supported on different materials [7–10]. Economic price, high activity and easy availability of nickel make it superior over the other metals. High nickel loading is usual in commercial supported catalysts [11]. Normal operating conditions in commercial batch reactors are temperature range: 120–200°C, pressure: 1–5 bar and catalyst loading ranging from 0.01 to 0.2 wt% depending on the properties of the final product [12, 13]. It is desired to maximize the amount of oleic acid (C18:1) in the final product, as well as to eliminate linolenic acid and to reduce the content of linoleic acid to a substantial extent, without going too far towards producing the fully saturated stearic acid (C18:0), since these are not easily digested as foodstuffs [14].

During partial hydrogenation, some of double bonds of unsaturated fatty acids in TAGs can be isomerized into *trans* fatty acids (TFAs). Their intake was convincingly associated with risk of coronary heart disease (CHD) based on epidemiologic and clinical studies and has been shown to be harmful to human health [15–17]. In the last three decades, numerous research works were published in order to explain the effect of TFAs on the cellular metabolism. The consumption of foods high in TFAs has been shown to increase LDL-C and decrease HDL-C levels, which increases the risk of developing CHD [18]. For this reason, the demand for smaller levels of TFAs content in hydrogenated oils has increased and the search for alternatives is important to improve the hydrogenation process. Improvements are required to find new types of hydrogenation catalysts [19–25], new technological solutions [26] and new directions in edible oil modification processes, involving interesterification, fractionation, or blending [27].

http://dx.doi.org/10.5772/66967

The major advances in finding solutions leading to the reduction of TFAs in hydrogenated oils have been achieved in the field of hydrogenation catalysts. In the last two decades, there has been a growing interest for nanosized structures in the range 1–20 nm in different fields of research [28]. This is also the size of metal particles in supported metal catalyst of new generation of nickel [19, 25, 29–31] and precious metal hydrogenation catalysts [20, 32–34]. In general, such nanoparticles of metals such as nickel, palladium, ruthenium, or platinum are used for hydrogenation, since the dissociatively adsorbed hydrogen is easily accessible on these group VIII metals. Supported metal catalysts containing both a group VIII and a group II metal [32, 35, 36], or a case where the catalysts containing both a group VIII and a group IB metal [22, 29, 37–40] although insufficiently studied, can be found in the literature. In these catalysts, the metal of group II or group IB is added as the modifier with the purpose of promoting the *cis*-isomer selectivity. Recently, systematic investigation has been performed over Pd-Mg, Pt-Mg and Ni-Mg supported on silica [36] and Ni-Mg-Ag supported on diatomite catalysts [29]. Regarding to *cis*/*trans*-selectivity, these catalysts produce less *trans* isomers, promoting the *cis*-selectivity. The results have been interpreted by implying electronic effect—modifying the local electron density of the transition metal either directly or through the support [36] or geometrical effect (two separate metal phases)—blocking or masking the effect on the active metal particles without forming the chemical bond [29].

Although many preparation methods have been developed for synthesis of a well-defined supported metal nanocatalyst, traditional precipitation methods remain widely used, especially for industrial applications, due to their relatively low cost and simplicity. These approaches typically involve precipitating of metal salts with an alkaline precipitant in the presence of suspended supports and then thermal decomposition of salt to yield a dispersion of metal particles on the support. It is often challenging to generate uniform metal dispersions, especially in the case of high metal loading in supported metal catalysts. The desired metal dispersion depends on different factors, including synthesis method, nature of the support, identity of metal precursor salt, concentration of the metal, prereduction treatment and reduction conditions [41–44].

The most common methods used for preparation of supported nickel catalysts include impregnation, co-precipitation and precipitation-deposition (PD). Among these methods, to prepare catalysts with high nickel loading, the most suitable is the PD method. However, in the synthesis of supported catalysts by this method, the interaction of the precipitating precursor with the support such as silica or alumina plays a dominant role. Nickel ions (Ni^{2+}) can react with hydroxyl ions and silica to form a bulk compound, nickel hydrosilicate, which is more stable than the bulk hydroxide or hydroxyl-carbonate and nuclei stabilized by interaction with silica surface [45, 46]. It is undoubtedly proven that the reason for the difficulty of reduction of the active phase on the supported metal catalyst lies in the strong mutual interaction between precipitating nickel precursors and the silica support, with at least partial formation of nickel hydrosilicates [46–49].

In the partial hydrogenation process of edible oils, a catalyst with the high activity and selectivity is required [50–52]. To meet these requirements, the catalyst support should provide sufficient surface area for the metal to disperse and there must be adequate metal-support interaction [35, 43, 46, 48, 49, 53–57]. The nickel phase on different support surfaces exhibits different extents of metal-support effects. This implies that the surface properties

of the catalyst could be changed by the nature of the supported Ni^{2+} phase, thus acquiring different characteristics and exhibiting different performances toward activity and selectivity, which are known to vary considerably with changes in the preparation conditions [41].

To control the fatty acid composition through temperature, pressure, catalyst and reaction time it is necessary to have a kinetic equation. The kinetic equations based on complex mechanisms as Horiuti-Polanyi [58] obtained from an extensive experimental work, give good results for predicting the reaction products, but in practice, simple mechanisms are employed with approximate results. An alternative is to use empirical modeling approach, which includes mathematical and statistical techniques for chosen empirical model [59–66].

The present work contains a part of our comprehensive research that we conducted on different nickel-based supported hydrogenation catalysts for their use in partial hydrogenation of edible oils. In this work, the characteristics and the structure of high loading nickel-based catalysts supported on diatomite, silica gel and perlite of different properties are related to their activity and selectivity in the hydrogenation of sunflower and soybean oils. Nitrogen physisorption and mercury porosimetry measurements, infrared and X-ray diffraction spectroscopy analyses, temperature programmed reduction studies, quantitative hydrogen chemisorption measurements and X-ray photoelectron spectroscopy were used. The kinetic models for hydrogenation of soybean and sunflower oils were developed to obtain the related kinetic parameters. The partial results derived of each one, treated together, have allowed us to present an overall picture of the nickel-based supported catalysts and some conclusions concerning the relationship in the triad—synthesis, structure and properties.

2. Experimental

2.1. Materials used

The support materials used for the synthesis of nickel-based catalysts were diatomite, silica gel and perlite. Diatomite support (D) was prepared from local crude diatomite (Baroševac-"Kolubara" coal basin, Lazarevac, Serbia) in our laboratories (IChTM-DCCE, see [67]). The crude material was mechanically, chemically and thermally treated to obtain the desired support characteristics. Three types of commercial silica gel with different textural characteristics (silica gel-A, silica gel-B, silica gel-C, silica gel = SiG hereinafter expressed as SiG-A, SiG-B and SiG-C, see [68]), produced in Bulgaria, were used for the preparation of the nickel-based catalyst supported on silica gel. Expanded perlite (PF, commercial product Perfit PF-295) supplied with the courtesy of Termika Zrenjanin, Serbia, was used for synthesis of nickel-based catalysts on perlite. Some of their characteristics are summarized in **Table 1**.

Refined, bleached and deodorized commercial sunflower oil (Dijamant AD Company, Zrenjanin, Serbia) along with refined and bleached soybean oil provided by Factory of Oils and Vegetable Fats Vital-Vrbas, Serbia, were used in the hydrogenation experiments. The initial iodine value (IV) and the fatty acid composition of sunflower and soybean oil are listed in **Table 2**.

http://dx.doi.org/10.5772/66967

Support	Property							
	Nitrogen physisorption[a]			Mercury porosimetry[b]				He-P[c]
	S_{BET} (m^2 g^{-1})	V_{micro} (cm^3 g^{-1})	V_{meso} (cm^3 g^{-1})	V_p (cm^3 g^{-1})	D_{mean} (nm)	ρ_{bulk} (g cm^{-3})	P (vol %)	ρ_{app} (g cm^{-3})
Diatomite (D)*	29	0.010	0.063	1.40	1188	0.59	73	2.21
Silica gel (SiG)*								
SiG-A	777	0.280	0.170	0.05	13	1.21	6	1.29
SiG-B	581	0.210	0.780	0.21	15	1.41	29	1.98
SiG-C	387	0.140	0.850	0.31	13	0.73	22	0.94
Perlite (PF)*	6	0.002	0.015	2.56	5500	0.25	89	2.23

*SiO2 content (wt%): Diatomite (D)—93.07; Silica gel (SiG-A, SiG-B, Sig-C)—100; Perlite (PF)—74.10.
[a]Determining surface area, adsorbed volume and pore size distribution in the micro- and mesopore ranges: S_{BET}—BET specific surface area; V_{micro}—specific pore volume (micropore range: D < 2nm); V_{meso}: specific pore volume (mesopore range: 2 nm < D < 50 nm).
[b]Determining total pore volume and pore size distribution in the meso- and macropore ranges: V_P—specific pore volume at 200 MPa; pore diameter: D_{mean}—mean pore diameter; P—total porosity; constant surface tension for Hg was assumed: γ = 480 dyn cm^{-1}.
[c]Helium picnometry—determining apparent density: ρ_{app}—includes closed pore (IUPAC).

Table 1. Typical catalyst support characteristics.

		Soybean oil (SBO)	Sunflower oil (SFO)
Iodine value (IV)		130.2	131.5
Fatty acid composition—CX:Y[b] (mass%)			
Palmitic	C16:0	11.0	7.3
Stearic	C18:0	4.5	4.0
Oleic	C18:1	21.3	26.0
Elaidic	C18:1*t*	< 0.1	< 0.1
Linoleic	C18:2	53.8	62.2
Trans acids sum[c]	*trans*-C18:2 sum	< 0.1	< 0.1
Linolenic	C18:3	7.1	< 0.1
Others	C14:0-C24:0 (soybean oil)	2.2	–
	C20:0-C22:0 (sunflower oil)	–	0.4

[a]Initial unsaturation of soybean and sunflower oil was measured in terms of IV.
[b]First number represents the total carbon number of the acyl groups and the second number represents the total number of double bounds.
[c]Sum: C18:2*c,t* + C18:2*t,c* + C18:2*t,t*.

Table 2. Iodine value (IV) and fatty acid composition of soybean and sunflower oils.

Analytical grade chemicals and pure hydrogen (99.999%) and nitrogen (99.999%) were employed in the experiments and none of these gases contained catalyst-poisoning substances such as oxygen or sulfur.

2.2. Catalyst preparation

Catalyst precursor synthesis. All catalyst precursors were prepared by the precipitation-deposition method. **Figure 1** shows a schematic of the experimental setup for catalyst precursor synthesis.

Table 3 lists catalyst precursor samples designation, synthesis operating parameters and nickel loadings.

The details of the synthesis procedures for differently supported nickel-based catalyst precursors were given in our earlier works [29, 69, 57, 31].

Catalyst precursor reduction. The reduction of the catalyst precursors was performed by a dry reduction method in a laboratory apparatus shown in **Figure 2** (line: reduction). Catalyst precursors were heated up to 430°C at a rate of 1.5°C min^{-1} under flowing H_2/N_2 gas mixture (150 cm^3 min^{-1}, 50 vol% of H_2) and maintained at 430°C for 5 h. Precursor treated in this way is referred to as Rp (e.g., $(Ni\text{-}Mg/D)_{Rp}$).

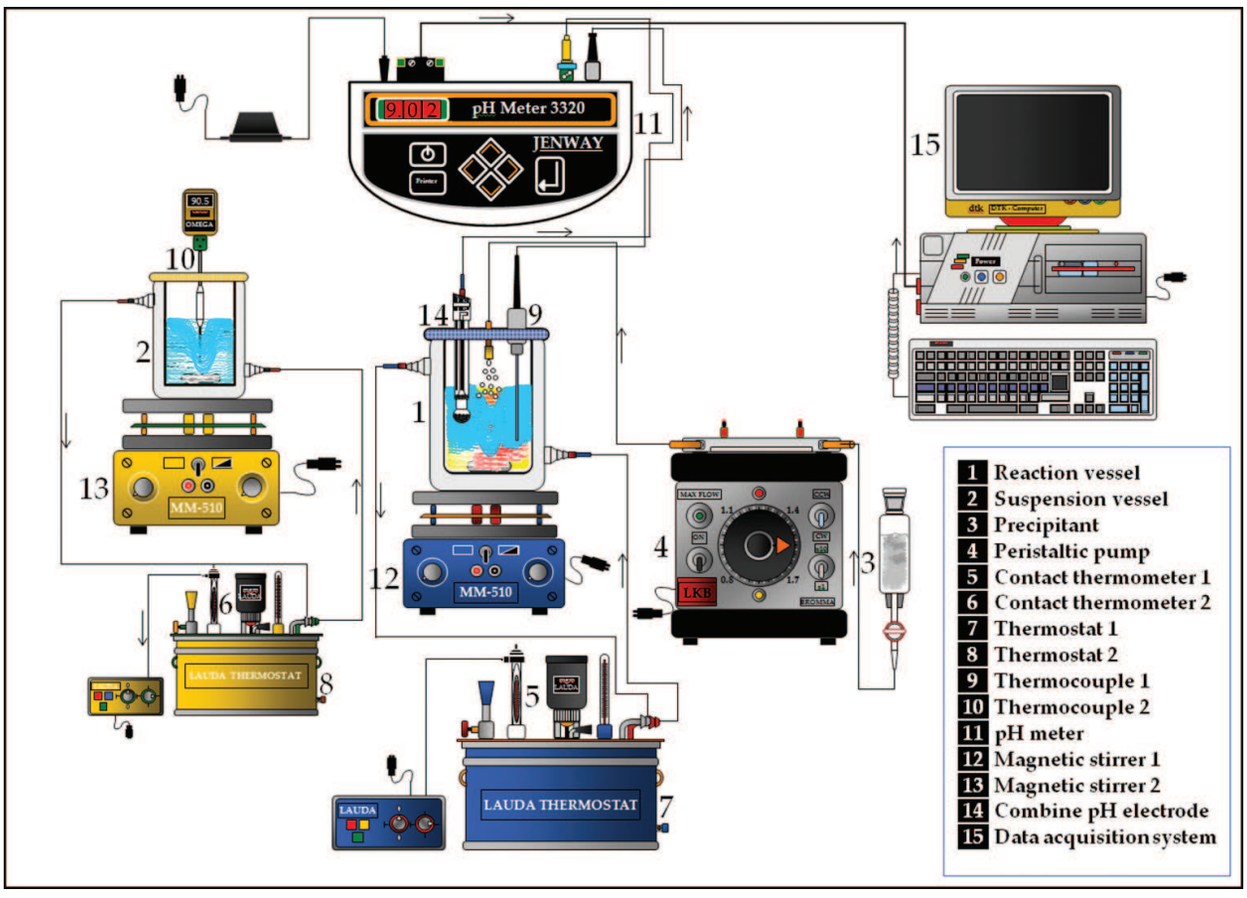

Figure 1. Schematic representation of the experimental setup—catalyst precursor synthesis.

Designation[a]		Synthesis operating parameters[b]				Ni loading
Catalyst precursor (system)	**Sample (code)**	**Ni/SiO_2 (molar ratio)**	**Ni/Mg[b] (atomic ratio)**	**T_{PD}[b] (°C)**	**t_{AG}[b] (min)**	**Ni (wt%)**
Ni-Mg/D	Ni-Mg/D*	0.93/1	10/1	90	120	36.3
	Ni_A-Mg/D	0.93/1	10/1	90	120	36.6
	Ni_C-Mg/D	0.93/1	10/1	90	120	36.2
	Ni_F-Mg/D	0.93/1	10/1	90	120	36.6
	Ni_S-Mg/D	0.93/1	10/1	90	120	35.0
Ni-Mg-Ag/D*	Ni-Mg-$Ag_{0.16}$/D*	0.93/1	10/1	90	120	35.9
	Ni-Mg-$Ag_{1.55}$/D*	0.93/1	10/1	90	120	35.2
	Ni-Mg-$Ag_{5.88}$/D*	0.93/1	10/1	90	120	33.5
Ni/SiG*	Ni/SiG-A*	1.01/1	–	90	120	43.7
	Ni/SiG-B*	1.11/1	–	90	120	45.5
	Ni/SiG-C*	1.00/1	–	90	120	43.5
Ni-Mg/PF*	Ni-Mg/PF-1*	1.00/1	10/1	90	30	30.2
	Ni-Mg/PF-2*	1.75/1	10/1	90	30	36.0

*Referred to catalyst precursors sample prepared from nitrate salts of nickel and modifier.

[a]Symbols in sample designation: A—acetate, C—chloride, F—formate, S—sulfamate; numbers refer to the Ag loading: 0.16 wt% of Ag (Ni-Mg-$Ag_{0.16}$/D), 1.55 wt% of Ag (Ni-Mg-$Ag_{1.55}$/D), 5.88 wt% of Ag (Ni-Mg-$Ag_{5.88}$/D); $Ni/Ag_{0.16}$ (atomic ratio) = 400/1, $Ni/Ag_{1.55}$ (atomic ratio) = 40/1, $Ni/Ag_{5.88}$ (atomic ratio) = 10/1.

[b]Constant parameters: T_{PD}—reaction temperature (precipitation-deposition), t_{AG}—aged temperature, precipitant: anhydrous Na_2CO_3 approx. 50% in excess with respect to a sum of Ni and Mg molar content.

Table 3. Catalyst precursor systems and samples prepared.

Reduced catalyst precursor soaking—final catalyst. After cooling down to room temperature, reduced catalyst precursors were protected by soaking in pure paraffin oil. After removing the excess of paraffin oil by filtering, the final catalyst was stored.

Reduced catalyst precursor passivation. Passivation of the reduced catalyst precursors was necessary to prevent the exceptional pyrophoricity of the metallic nickel before the reduced precursor was exposed to air for characterization and handling. This treatment was carried out in a laboratory apparatus depicted in **Figure 2** (line: passivation). Reduced catalyst precursor was passivated at room temperature in a N_2 stream (150 cm^3 min^{-1}) containing 350 ppm O_2 for 30 min.

2.3. Characterization

Chemical analyses. The chemical analysis of nickel (Ni) was performed by standard test methods for quantitative analysis (dimethylglyoxime method). The silver (Ag) loading was determined using inductively coupled plasma-optical emission spectroscopy (ICP-OES) on an iCAP 6500 Duo apparatus (Thermo Fisher Scientific). Before the analysis, the precursors were subjected to microwave digestion using a Milestone Ethos 1 advanced microwave digestion system.

Nitrogen physisorption (N_2-physisorption). N_2 adsorption/desorption isotherms of the catalyst precursors at −196°C were measured on a Thermo Finnigan Sorptomatic 1990. Precursors

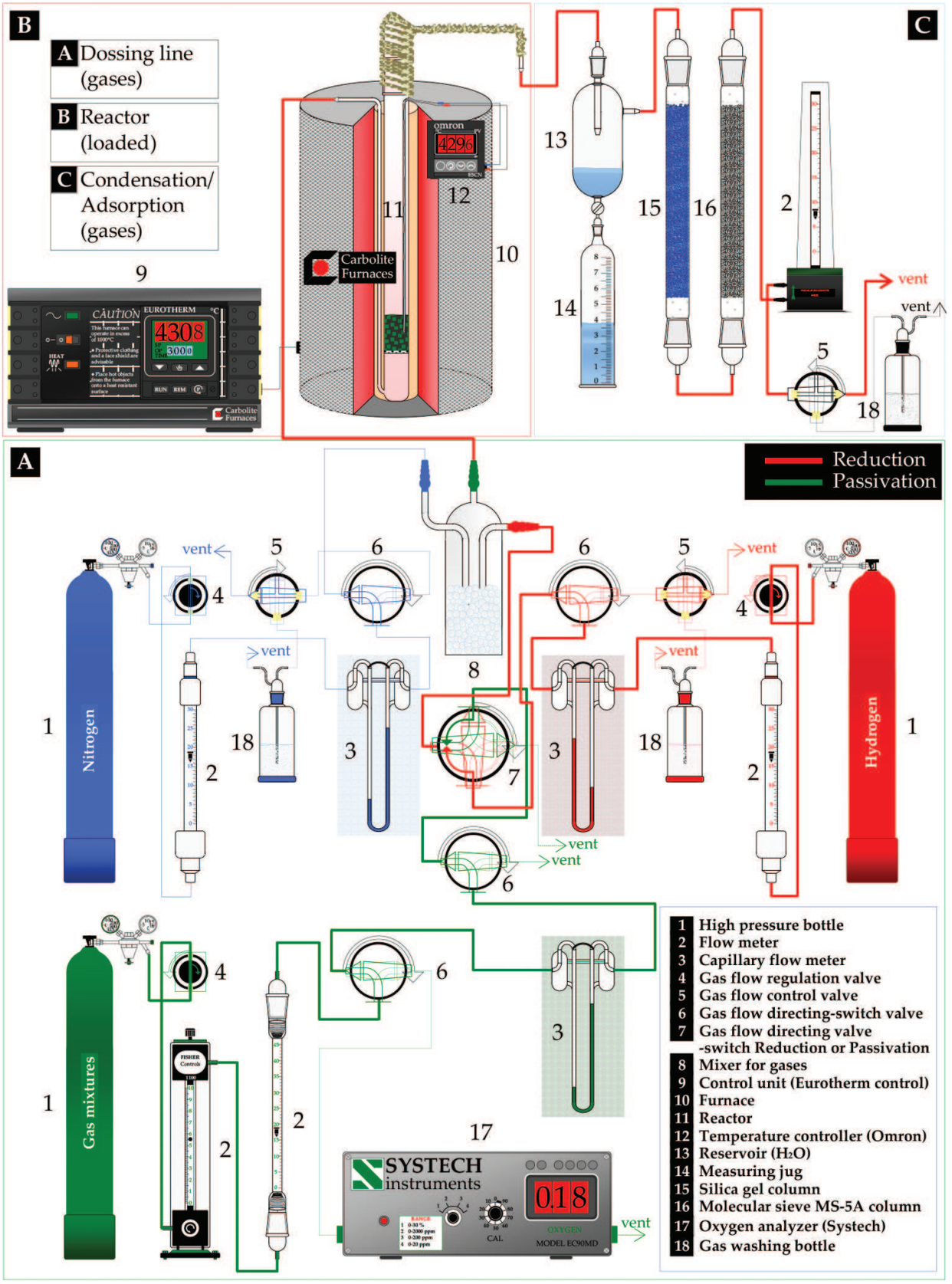

Figure 2. Schematic representation of the experimental setup—catalyst precursor reduction/passivation.

http://dx.doi.org/10.5772/66967

were previously degassed for 16 h at 110°C and 10^{-3} Torr (1 Torr = 133.3 Pa). The BET equation was used to calculate the specific surface area, S_{BET}. Total pore volume, V_p, was estimated at a relative pressure of 0.99.

Mercury porosimetry (Hg-porosimetry). Hg-porosimetry measurements were performed in the fully automated conventional porosimeters: 1. Thermo Scientific Pascal 140 porosimeter (pressure range: 0.01–0.1(0.4) MPa; pore size (diameter) range: 3.8–116 μm); 2. Thermo Scientific Pascal 440 porosimeter—Solid 1.3.4 software (pressure range: 0.1–400 MPa; pore size (diameter) range: 0.0036–15 μm)—data acquisition with the software package Solid 1.3.4; 3. Carlo Erba Macropore 120 porosimeter (pressure range: 0.01–0.1 MPa; pore size (diameter) range: 3.8–116 μm (or 15–150 μm); 4. Carlo Erba 2000 porosimeter (pressure range: 0.1–200 MPa; pore size (diameter) range: 0.0075–15 μm)—data acquisition with the software package Milestone 200.

Density measurements. Apparent densities were measured using a helium pycnometer, which uses a gas displacement technique to determine the volume of the solid material under test. The measurements were performed using a Pycnomatic ATC (Thermo Fisher Scientific).

IR measurements. IR spectra were recorded on a Perkin Elmer 983 G spectrometer (4000–250 cm^{-1}) and a Thermo Scientific Fourier transform Nicolet 6700 spectrometer (4000–400 cm^{-1}). KBr pellet method was used: 1 mg of precursor was well mixed into 200 mg fine KBr powder and the finely pulverized and put into a pellet-forming die.

X-ray diffraction (XRD). Powder XRD patterns were obtained with a Siemens D5005 diffractometer, equipped with a graphite monochromator and Antoan Paar chamber. Copper filtered Cu Kα radiation (λ = 0.154184 nm) was employed covering 2θ angles from 5 to 80° or from 10 to 100°. The average metal crystallite sizes were estimated by application of the Sherrer equation. The width of the Ni-(111) peak at half-maximum was corrected for Kα doublet and instrumental broadening.

Hydrogen temperature programmed reduction (H_2-TPR). Hydrogen temperature programmed reduction experiments were carried out in an automatic apparatus Thermo Scientific TPDRO, Pulse Chemisorb 1100. H_2-TPR experiments of catalyst precursors were performed in the temperature range 50-900°C, using a flow of H_2/Ar (20 cm^3 min^{-1}, 4.9 vol% of H_2) and a heating rate of 2°C min^{-1}. A cooling trap filled with 3A-MS was installed between the oven and TCD to remove the water formed during the reduction. The consumption of H_2 was monitored by a thermal conductivity detector. The detector response was calibrated by reducing a known mass of CuO. TPR profiles were normalized to the same mass of catalyst precursors.

Hydrogen chemisorption (H_2-chemisorption). H_2-chemisorption data were obtained using both the static method (standard volumetric apparatus) and the dynamic method (Thermo Scientific TPDRO, Pulse Chemisorb 1100).

Experimental setup—standard volumetric apparatus. In situ reduction of catalyst precursors at 430°C for 1 h by passing a mixture of hydrogen and nitrogen (H_2/N_2 = 1:1 v/v) over the sample. Reduction conditions were as follows: heating rate: 2°C min^{-1} and H_2/N_2 gas mixture flow of 20 cm^3 min^{-1}. After reduction, the precursors were degassed at 10^{-4} Pa for 4 h at the same temperature and cooled at 25°C to carry out chemisorption measurements. The pressure range of the isotherms was 0.1–13.3 kPa and the amounts of hydrogen chemisorbed were calculated by

extrapolation of the isotherms to zero pressure. Further details about the expressions used to calculate nickel crystallite sizes can be found in our previous paper (see [29]).

Experimental setup—pulse chemisorb TPDRO 1100. In situ reduction of catalyst precursors at 430°C (2°C min^{-1}) for 1 h, under a flow of 20 cm^3 min^{-1} H_2/Ar (4.9 vol% of H_2). After reduction, the precursors were degassed by temperature programmed desorption at 425°C (carrier gas Ar) and cooled at 45°C, to carry out chemisorption of H_2. Finally, the catalyst precursors were subjected to a known number of calibrated pulses (0.353 cm^3) of pure H_2 at 45°C.

X-ray photoelectron spectroscopy (XPS). The quantitative chemical composition of surfaces of catalyst precursors and the valence state of studied ions were obtained by X-ray photoelectron spectroscopy. XPS measurements were performed using a VG Scientific Escalab Mk II spectrometer interfaced with the necessary data handling software Lab Cal 2. Spectra were recorded under ultrahigh vacuum conditions (10^{-8} Torr), using Al Kα primary radiation (1486.6 eV). Data were collected in the sequence of a survey scan (to determine the C 1s reference), followed by scans of the O 1s, S 2p, Ni $2p_{3/2}$ and Ag 3d regions to minimize the time of exposure to X-rays.

2.4. Catalytic activity measurements

Partial hydrogenation of sunflower and soybean oil over prepared catalysts was carried out under laboratory and pilot plant conditions. Schematics of the lab- and pilot-experimental setup are shown in **Figures 3** and **4**.

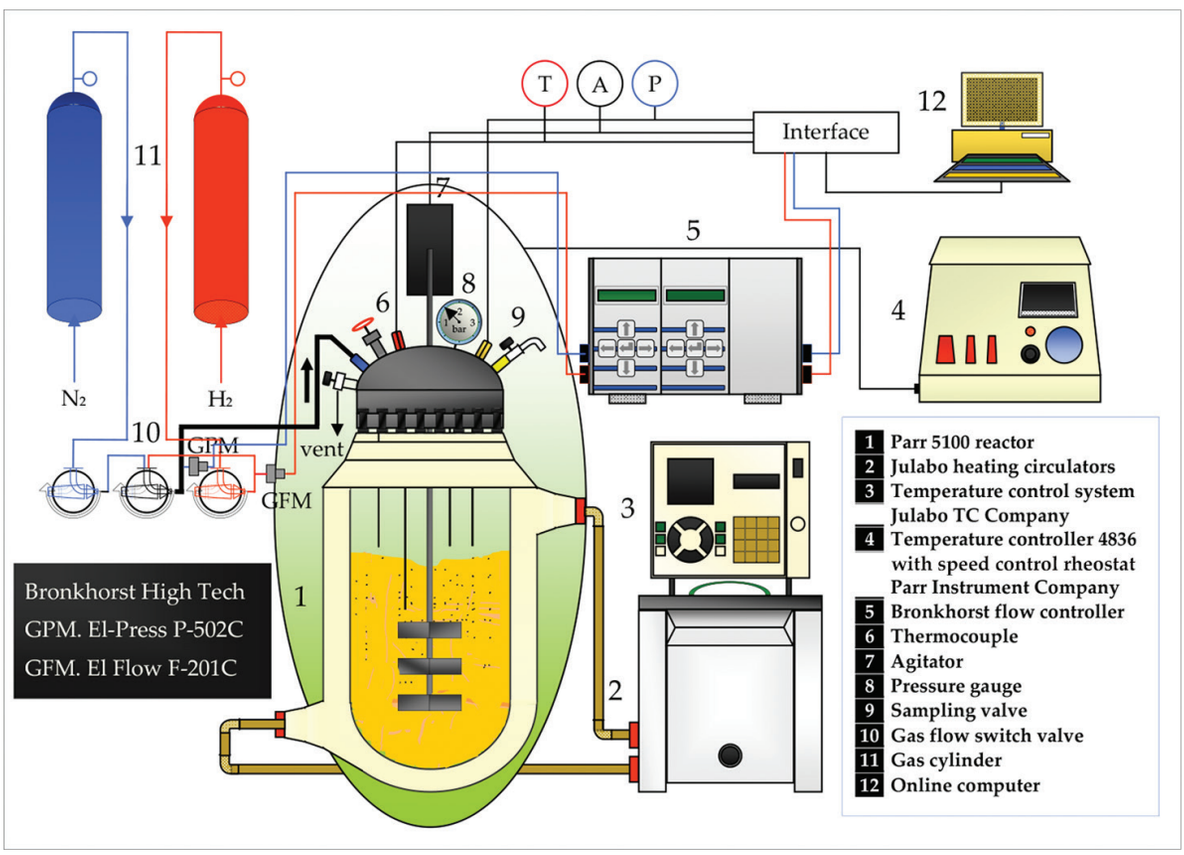

Figure 3. Schematic representation of the experimental setup—laboratory reactor system.

http://dx.doi.org/10.5772/66967

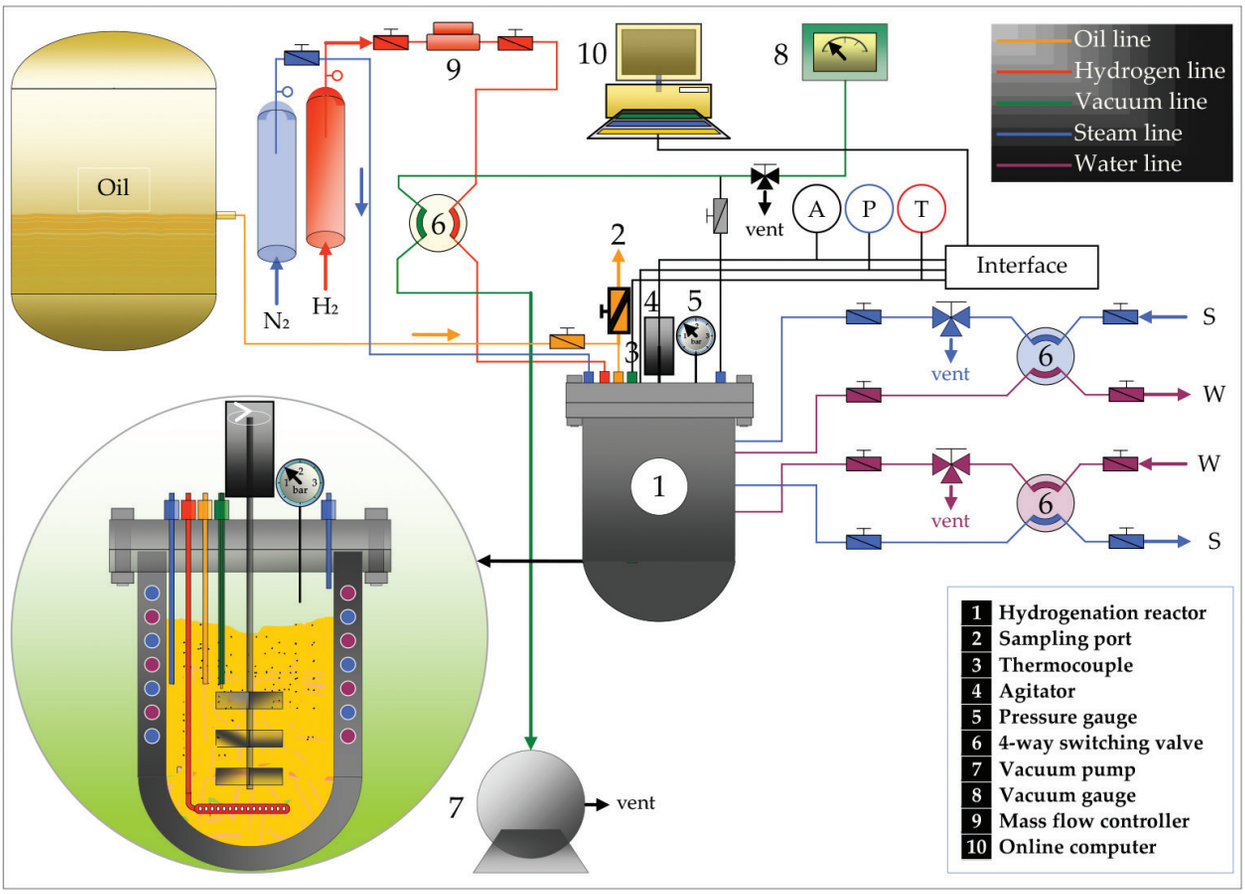

Figure 4. Schematic representation of the experimental setup—pilot plant reactor system.

Experimental setup—laboratory reactor system. The hydrogenation tests were carried out in a Parr 5100 glass 1 L jacketed reactor operated in a semibatch mode. The laboratory system comprises a catalytic reactor interfaced with a mass flow controller—Bronkhorst EL-FLOW model F-201C and a digital electronic pressure meter—Bronkhorst EL-PRESS model P-502C and a minicomputer. The reactor was connected to a hydrogen source, maintained at a constant pressure. The reduced catalyst was added to the oil when the reaction temperature was reached using a new type of catalyst feeder constructed in our laboratories (IChTM-DCCE). The catalytic tests were performed at 160°C and 0.2 MPa, using 900 g of sunflower oil. The catalyst weight was adjusted in order to keep constant oil to Ni mass ratio (0.06 wt% Ni with respect to the amount of oil). The stirring rate was 1200 rpm. An experimental procedure of hydrogenation test under laboratory conditions was described in detail in our previous paper [30].

Experimental setup—pilot plant reactor system. The catalytic experiments were carried out in a 7.5-L batch-stirred PPV (Pilot Plant Vital) reaction vessel. The PPV and its ancillaries were available at the research facilities of Oils and Vegetable Fats Factory Vital-Vrbas. **Figure 4** shows a schematic representation of the experimental setup.

Each experiment was performed at a constant liquid volume and constant oil/catalyst mass ratio (see [29]). Before the reactor was heated, the headspace was purged with nitrogen to remove oxygen. The catalyst sample was precisely weighed and added to the liquid soybean oil at working temperature (160°C), under a mixing speed set at 750 rpm. The reactor was

then pressurized with pure hydrogen to the operating pressure (0.16 MPa). During the experiments, the heat flow, hydrogen uptake and reactor temperature and pressure were monitored by instruments interfaced to the reactor PPV system. For each run, the soybean oil batch was partially hydrogenated to a final IV of 90. The composition of fatty acids in the original soybean oil and hydrogenated products was analyzed by the capillary gas chromatographic method. Experiments were performed on a Schimadzu GC-9A equipped with flame ionization detector (FID). Chromatographic conditions were as follows: HP-88 capillary column (100 m × 0.25 mm, 0.20 μm film thickness, Agilent), oven temperature of 180°C, detector and injector temperature of 240°C. Injection was carried out in the splite mode at a splite ratio of 1:4. The injection volume was 2 μL. Helium was used as the carrier gas at a constant flow rate of 1.2 $cm^3\ min^{-1}$. The IUPAC method II.D.19 [70] for preparation and CG analysis of fatty acids methyl esters was used to convert fatty acids, taken out at predetermined time intervals from the catalytic reactor, into their corresponding methyl esters.

3. Results and discussion

3.1. Catalyst precursor characterization

Nitrogen physisorption (N_2-physisorption—NP). Nitrogen adsorption-desorption measurements were performed to determine the effect of the support and preparation parameters on the BET surface area, pore volume and mean pore diameter of prepared catalyst precursor samples. The obtained results are summarized in **Table 4**.

Table 4 reveals that specific surface area (S_{BET}) was greatly enhanced after deposition Ni^{2+} precipitates onto the macroporous diatomite and/or perlite support. The prepared samples have BET surface areas, which are an order of magnitude larger than the surface area of the supports. The catalyst precursors have significantly different values of the pore volume and mean diameter of pores compared to the starting support materials (**Tables 1** and **4**). It has been shown in numerous studies that improved textural properties of the supported metal catalysts are related to the metal-support interaction (MSI) [49, 71–73]. This phenomenon was also observed in the nickel catalysts supported on diatomite and/or silica [54, 71]. The authors explained an extremely enhanced BET surface area by forming supported intermediate phases layered structure-nickel hydrosilicates as a result of nickel-support interaction. Nepouite-like (1:1 nickel hydrosilicate) is the main Ni^{2+} phase formed in Ni/SiO_2 samples prepared by the PD method on silica with a high surface area [56]. In the case of Ni-Mg/D precursors, it is reasonable to assume that the improved textural properties of the precursors are the results of MSI, as elucidated by IR and XRD patterns discussed later in this paper. Ni/SiG precursors showed different behavior. A considerable decrease in the BET surface area was observed in the Ni/SiG-A and Ni/SiG-B precursors formed by precipitating the Ni^{2+} species onto micro- (SiG-A) and mesoporous (SiG-B) supports initially having high surface areas. It is well known that the supports with low specific surface areas favor the formation of nickel hydroxide or hydroxyl-carbonate phases whatever the preparation method is, while supports with high specific surface areas allow the growth of hydrosilicate to occur [74]. It is likely that the high nickel loadings in those precursors (above 40 wt%, **Table 3**)

Sample	S^a ($m^2\ g^{-1}$)	S_{meso}/S^b	V_p ($cm^3\ g^{-1}$)	$V_{meso}/V_p{}^b$	$D_{mean}{}^c$ (nm)
Ni-Mg/D	224	0.602	0.201	0.695	3.5
Ni_A-Mg/D	223	0.430	0.161	0.571	3.7
Ni_C-Mg/D	208	0.516	0.170	0.694	4.1
Ni_F-Mg/D	177	0.477	0.150	0.613	4.5
Ni_S-Mg/D	255	0.472	0.232	0.698	5.5
Ni-Mg-$Ag_{1.55}$/D	167 (157*)	0.655 (0.585*)	0.172 (0.157*)	0.610 (0.599*)	4.1 (4.0*)
Ni-Mg-$Ag_{5.88}$/D	124 (136*)	0.812 (0.753*)	0.149 (0.157*)	0.691 (0.662*)	4.8 (4.6*)
Ni/SiG-A	269 (146*)	0.781 (0.836*)	0.530 (0.310*)	0.604 (0.710*)	8.8 (8.9*)
Ni/SiG-B	392 (193*)	0.735 (0.642*)	0.840 (0.320*)	0.464 (0.594*)	6.7 (7.0*)
Ni/SiG-C	367 (216*)	0.757 (0.676*)	0.630 (0.340*)	0.730 (0.647*)	10.2 (7.0*)
Ni-Mg/PF-1	210	0.622	0.169	0.799	3.7
Ni-Mg/PF-2	225	0.898	0.186	0.946	3.6

*Data for reduced-passivated samples: $(Ni\text{-}Mg/D)_{Rp}$, $(Ni\text{-}Mg\text{-}Ag_{1.55}/D)_{Rp}$ and $(Ni\text{-}Mg\text{-}Ag_{5.88}/D)_{Rp}$; $(Ni/SiG\text{-}A)_{Rp}$, $(Ni/SiG\text{-}B)_{Rp}$ and $(Ni/SiG\text{-}C)_{Rp}$.
[a]S: specific surface area-BET method.
[b]S_{meso} and V_{meso}: contribution of the mesopores.
[c]D_{mean}: mean pore diameter.

Table 4. Nitrogen physisorption data for dried and selected reduced-passivated catalyst precursor samples.

mitigate the effect of MSI leading to the formation of bulk nickel hydroxyl-carbonate covering the hydrosilicate layer formed in MSI. On the other hand, the precipitation of Ni^{2+} species onto the SiG-C support does not affect the BET surface area of the Ni/SiG-C precursor (see **Tables 1** and **4**).

The nitrogen adsorption-desorption isotherms are presented in **Figure 5**. Comparative plots have been constructed for all supports and systems of catalyst precursors.

In general, the experimental N_2 adsorption-desorption curves of samples closely resemble a type IV isotherm characteristic for mesoporous solids according to the IUPAC classification, with exception of the samples of D and SiG-A that appear to be extensively macroporous (isotherm type II) and microporous (isotherm type I). In the case of catalyst precursors of type Ni-Mg/D (**Figure 5a** and **d**) after saturation of micropores, nitrogen uptake monotonically increases with p/p_0 values due to sorption in the sample larger pores. After filling of mesopores, the uptake remains essentially invariant with p/p_0 values. The slope of curves is small, indicating a low content of mesopores having a wide pore size distribution (PSDs). In contrast, the catalyst precursors prepared on SiG and PF supports had sharper slope of nitrogen adsorption curves, indicating mesopores present with narrow PSDs.

It is well known that the occurrence of the capillary hysteresis loop depends on the pore sizes. In N_2-physisorption, the isotherms of the samples with the smallest pore size do not exhibit hysteresis, while the samples with the smaller pore sizes exhibit isotherms with narrow hysteresis.

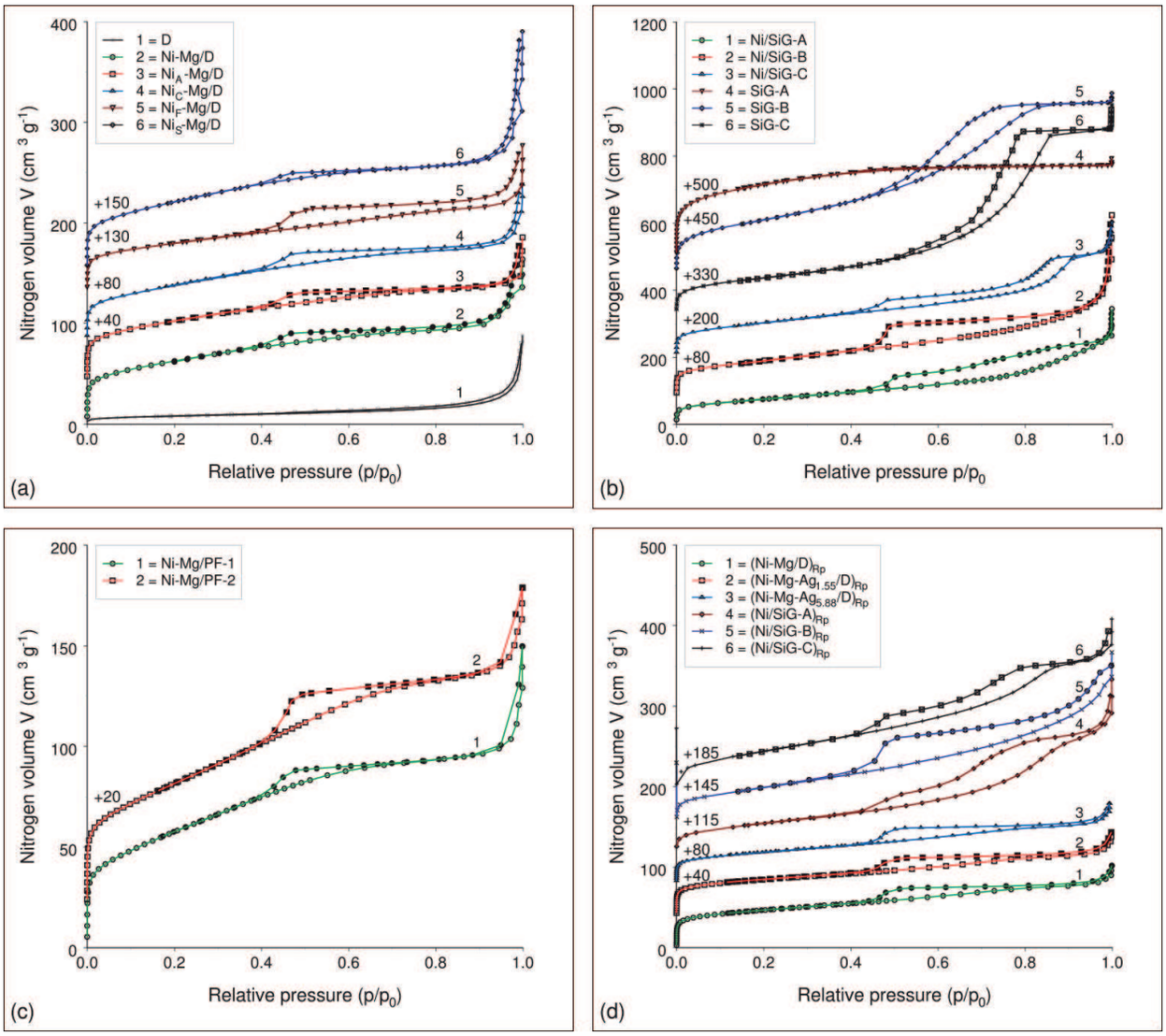

Figure 5. Experimental N_2 adsorption-desorption isotherms at -196°C for dried and reduced-passivated samples: (a) D, Ni-Mg/D; (b) SiG, Ni/SiG; (c) PF, Ni-Mg/PF; (d) $(Ni\text{-}Mg/D)_{Rp}$, $(Ni\text{-}Mg\text{-}Ag/D)_{Rp}$, $(Ni/SiG)_{Rp}$. Units and shifts along Y axis are chosen for convenience.

Wider capillary hysteresis loops are observed in the nitrogen isotherms on the samples with larger pore sizes. Besides, the shapes of the capillary hysteresis loops vary from a "triangle" to a well-pronounced "parallelogram". The results obtained for N_2-physisorption showed that samples differ in the shape and types of hysteresis. As can be observed, the precursors Ni-Mg/D, Ni-Mg-Ag/D and Ni-Mg/PF are characterized by capillary hysteresis loops with shape of a triangle (**Figure 5a** and **c**) unlike the precursor Ni/SiG having capillary hysteresis loops shape that look like a parallelogram (**Figure 5b**). The hysteresis type of the samples cannot be classified into any types of IUPAC classification and mostly resembles the H3 type corresponding to the mesoporous solids with a broad distribution of the pore sizes. Despite the expected absence of hysteresis for the diatomite support, a narrow loop of H1 type in the IUPAC classification was observed (**Figure 5a**).

http://dx.doi.org/10.5772/66967

Thermal treatment of reduced samples has not changed the pore structure significantly, preserving their mesoporosity (**Figure 5d**).

Mercury porosimetry (Hg-porosimetry—MP). The relevant mercury porosimetry experimental data are summarized in **Table 5**.

Table 5 indicates a large total pore volume and porosity for the dried catalyst precursor of Ni/SiG and Ni-Mg/PF systems. In the case of Ni-Mg/D catalyst precursor, the pore volume and porosity, as shown in **Table 5**, are obviously different from those mentioned above. The total pore volume and porosity are, in general, significantly lower and the pores are significantly smaller in diameter (D_{mean} and/or D_{av}). The differences between the prepared precursors may be associated with differences in pore structure characteristics of supports and the nature of nickel precursor salt.

Sample	V_p [b] ($cm^3\ g^{-1}$)	P[c] (vol %)	ρ_{bulk} [d] ($g\ cm^{-3}$)	D_{mean} [e] (nm)	D_{av} [f] (nm)
Ni-Mg/D	0.393	47	1.19	164	7.0
Ni_A-Mg/D	0.228	34	1.48	219	4.1
Ni_C-Mg/D	0.246	34	1.39	177	4.7
Ni_F-Mg/D	0.118	20	1.72	73	2.7
Ni_S-Mg/D	0.585	54	0.93	229	9.2
Ni-Mg-$Ag_{1.55}$/D	0.092 (0.135*)	16 (26*)	1.78 (1.89*)	29 (177*)	2.2 (3.4*)
Ni-Mg-$Ag_{5.88}$/D	0.111 (0.144*)	21 (29*)	1.84 (2.01*)	89 (189*)	3.6 (4.2*)
Ni/SIG-A	0.655	49	0.75	2331	9.7
Ni/SIG-B	1.876	72	0.38	1152	19.1
Ni/SIG-C	1.268	61	0.48	3087	13.8
Ni-Mg/PF-1	1.683	79	0.47	3690	32.0
Ni-Mg/PF-2	0.945	66	0.70	2237	16.8

*Data for reduced-passivated samples: $(Ni\text{-}Mg/D)_{Rp}$, $(Ni\text{-}Mg\text{-}Ag_{1.55}/D)_{Rp}$ and $(Ni\text{-}Mg\text{-}Ag_{5.88}/D)_{Rp}$.
[a]Acquisition data obtained by Milestone 200 and Pascal softwares.
[b]Pore volume.
[c]Porosity calculated from bulk density of dried sample as measured in porosimeter.
[d]Bulk density.
[e]Pore diameter: D_{mean}—computed from the corresponding PSD curves.
[f]Pore diameter: D_{av}—average pore diameter calculated according to the $D_{av}=4V_p/S_{BET}$ assuming cylindrical pore shape.

Table 5. Mercury porosimetry data for dried and selected reduced-passivated catalyst precursor samples[a].

The experimental PSDs data are presented in the form of cumulative pore diameters distribution curves in **Figure 6**. The data are cumulated from larger pore diameters measured to the smallest diameter limit set by the pressuring capacity of the instrument. According to the hysteresis curves (not shown), the main part of mercury remains in the pores after the measurement, indicating the presence of ink bottle-like pores.

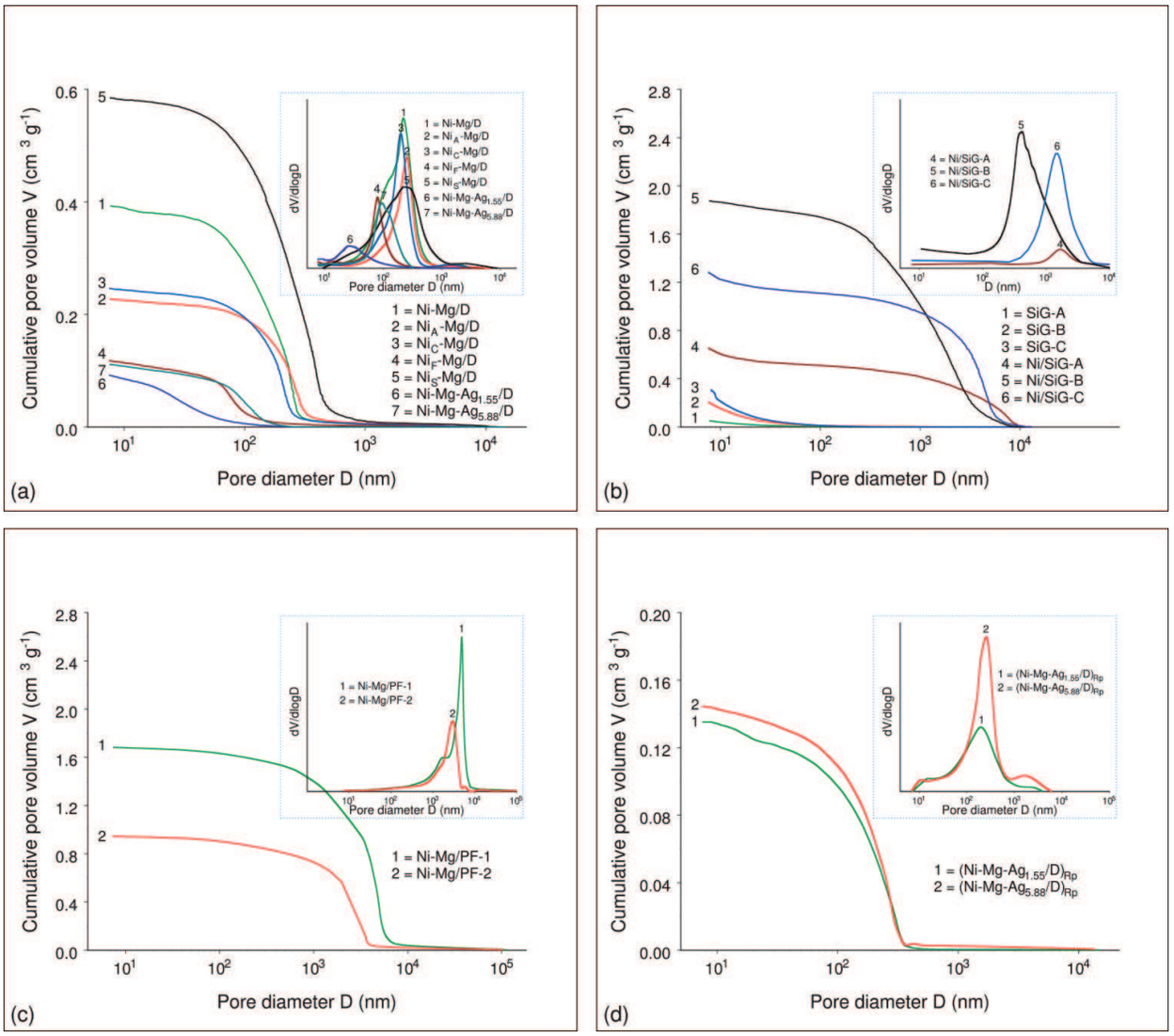

Figure 6. Cumulative and derivative PSDs for the SiG supports and catalyst precursor systems: (a) Ni-Mg/D, Ni-Mg-Ag/D; (b) SiG, Ni/SiG; (c) Ni-Mg/PF; (d) $(Ni\text{-}Mg\text{-}Ag/D)_{Rp}$.

The derivate distribution function (dV/dlogD) is represented as insert (see **Figure 6a–d**). It should be noted that the pressurization data from mercury intrusion yields information about the size of the opening of pores and/or voids and does not reflect the pore size behind the "neck". It is apparent that the deposition of Ni^{2+} precipitates onto surface of SiG supports leading to a shift in the PSD curves towards the larger pore diameters. The explanation for this effect appears to lie in different microstructural arrangements of supported Ni^{2+} species in dried samples compared to the starting supports (**Figure 6b**). Thermal treatment has led to opening of smaller pores and a slight displacement of PSDs to larger pore diameters (**Table 5**, **Figure 6d**).

Combined nitrogen physisorption and mercury porosimetry studies showed that all catalyst precursors had good textural properties, namely a high specific surface area and a well-developed porous structure, containing mesopores stable to thermal treatments. Mesoporosity

http://dx.doi.org/10.5772/66967

(pore width of 2–50 nm) is preferable for application that involves the liquid phase since it provides a balance between good diffusion rates of reactants and useful in-pore effects.

IR analysis. The IR method was employed to identify the Ni^{2+} species in the precursor samples. The identification of Ni^{2+} species by IR analysis is made by the comparison with reference bulk compound—basic nickel carbonate (BNC). **Figure 7** shows infrared and Fourier transform infrared spectra of the studied samples. The 2000–400 cm^{-1} region has been presented in order to obtain a better representation.

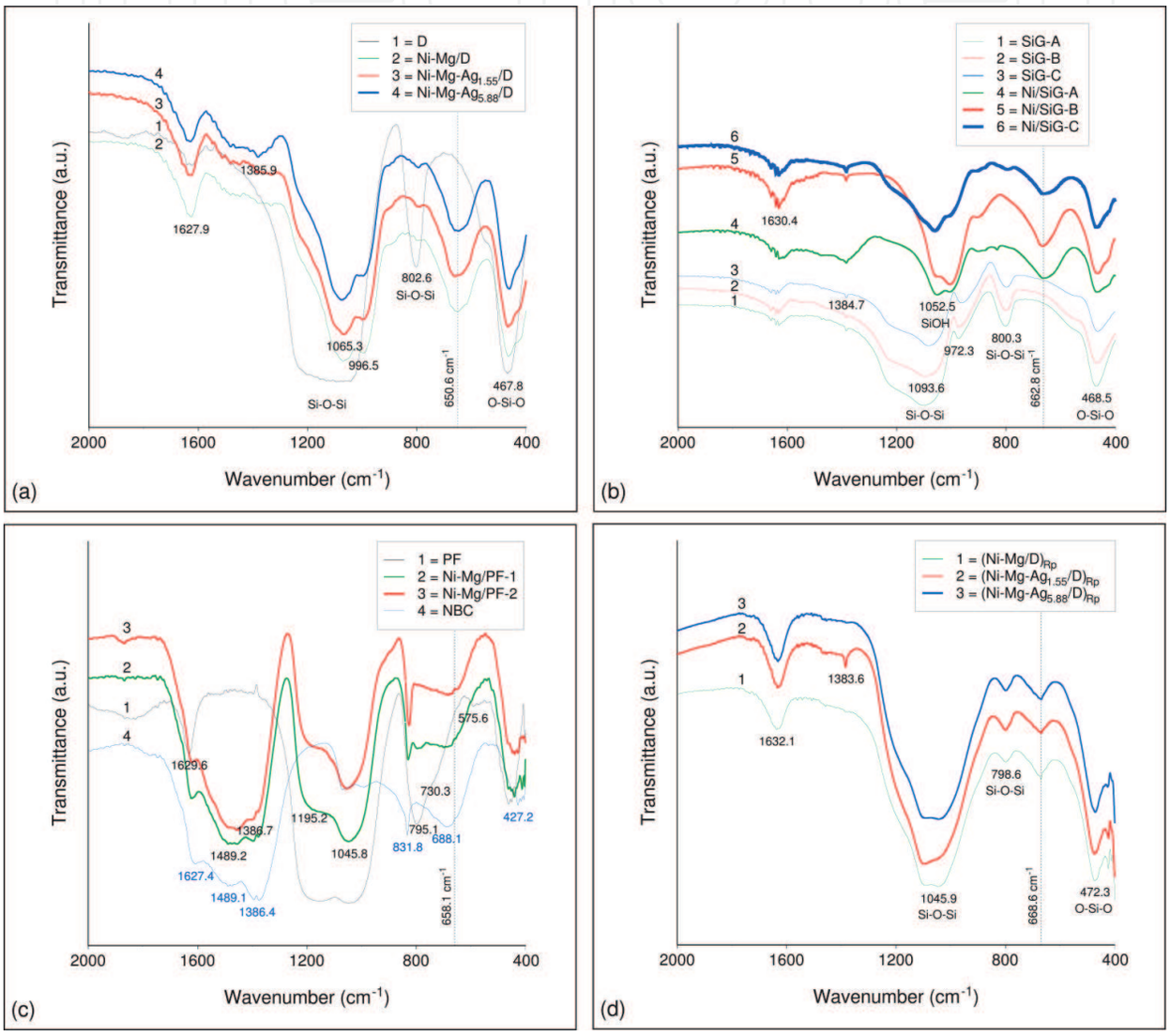

Figure 7. IR spectra of the supports and catalyst precursor samples: (a) D, Ni-Mg/D, Ni-Mg-Ag/D; (b) SiG, Ni/SiG; (c) PF, Ni-Mg/PF; (d) $(Ni\text{-}Mg\text{-}Ag/D)_{Rp}$. Units and shifts along Y-axis are chosen for convenience.

The infrared spectra of the D support and dried Ni-Mg/D catalyst precursors are shown in **Figure 7a**. The IR spectrum of the D support having silica as its main constituent ingredient shows antisymmetric stretching vibration band at around 1090 cm^{-1} and symmetric stretching vibration band at around 800 cm^{-1} characteristic for the Si-O-Si bonds [75]. The band at

around 470 cm^{-1} is associated with O-Si-O bond bending vibrations. The absorption band at around 1630 cm^{-1} can be assigned to the vibration of adsorbed molecular water.

IR spectra of precursors are similar to the spectrum of diatomite in the OH-stretching region containing vibration bands of silica-free hydroxyl groups, hydrogen-bonded hydroxyl groups and adsorbed molecular water (not shown in **Figure 7a**). The main absorption broad band in the spectrum of diatomite (1090 cm^{-1}) in the IR spectra of the precursors appeared to be composed of multiple bands around 1100 cm^{-1}. It can be observed the presence of three bands: IR band characteristic of silica at 1090 cm^{-1} was reduced to a shoulder, IR band characteristic of silicate-type species connected/interacted with carbonate rich BNC species appeared at 1065 cm^{-1} and shoulder appeared around 1000 cm^{-1} which could be attributed to silicate-type species connected/interacted with hydroxide rich BNC species [54]. The presence of intercalated anionic species in the Ni^{2+} precipitates is attested by the existence of bands at around 1630 cm^{-1} and at around 1385 cm^{-1} may be attributed to adsorbed molecular water and carbonate ions. By comparing spectra of precursors and diatomite, it can be observed that IR spectra of precursors contain a band at 650.6 cm^{-1} (**Figure 7a**) which does not exist in the IR spectrum of the diatomite support. The appearance of a new phase can be attributed to nickel hydrosilicates arisen from the interaction between nickel and the diatomite support. It is apparent that this method of preparation leads to extensive interaction between Ni ions and silica, presumably because under alkaline conditions the silica have a tendency to dissolve. Characterization studies have shown that Ni^{2+} precipitates on silica as layered nickel hydrosilicate [45–49, 53–57, 68, 72, 74]. In support of this claim is the fact that samples are prepared by a precipitation-deposition method, which leads to the formation of supported nickel hydrosilicates.

The IR spectra of SiG supports and Ni/SiG precursor samples are shown in **Figure 7b**. It is obvious that the IR spectra of these samples resemble those prepared with diatomite support (**Figure 7a** and **b**). This result was expected, having in mind the proportion of the SiO_2 component in the chemical composition of diatomite and SiG supports. In addition, a band at 972 cm^{-1} can be observed in all three types of SiG support. The band at around 970 cm^{-1} has been widely used to characterize the incorporation of metal ions in the silica framework as the stretching Si-O vibration mode perturbed by the neighboring metal ions. A new band at 662.8 cm^{-1} attributable to nickel hydrosilicates can also be observed in all Ni/SiG precursor samples (**Figure 7b**).

FT-IR spectra of the perlite support and Ni-Mg/PF precursors are presented in **Figure 7c**. The spectrum of perlite support in the region from 400 to 2000 cm^{-1} shows the presence of the main absorption structures, an intense band at about 1045 cm^{-1} with a shoulder at about 1200 cm^{-1}. These two bands are attributed to Si-O-Si and Si-O-M anti-symmetric stretching vibrations, where M can be Al or Si. A further group of three bands of medium intensity is present at lower wavelengths: 795, 730 and 575 cm^{-1}. The band at 795 cm^{-1} is assigned to symmetric stretching of Si-O-Si, at 730 cm^{-1} to bending Si-O-Al and at 575 cm^{-1} to symmetric stretching of Si-O-R [76]. Water molecule deformation vibrations at around 1630 cm^{-1} are also registered. The well-expressed bands at 1387 and 1489 cm^{-1} in the IR spectrum of precursors are attributed to the presence of an additional carbonate containing phase, most probably

located on the surface of the support. Comparing bands gained in synthesized precursors are apparent evidence of the created Ni^{2+} species on the support surfaces. On the reference sample spectra, existence of broad antisymmetric band at 688 cm^{-1} is evident. This band also exists in spectra of precursors, although slightly shifted towards lower wavenumbers with minimum at around 658 cm^{-1} (**Figure 7c**). Shift indicates a new type of interaction with the support, compared to the reference material and may be attributed to the Ni-O-Si vibrations [77]. It can also be stated that no evidence of structural change among the dried precursors can be acknowledged.

The IR spectra of precursors after the reduction treatment are presented in **Figure 7d**. The thermal treatment produced the elimination of adsorbed molecular water and carbon dioxide. The absence of silanol groups, as attested by disappearance of the anti-symmetric band at 980 cm^{-1} is clearly evident. Besides, a low intense band at 668 cm^{-1} indicates the presence of nonreduced silicate species in smaller amounts than in the dried samples (**Figure 7a** and **d**).

From the above results and with the available information in the literature, it could be concluded that during the deposition reaction under alkaline conditions, the silica as a constitutive component of all studied supports reacts with the basic nickel carbonate precipitate and generates the new supported nickel hydrosilicate phase containing Si-O-Ni linkages.

Powder X-ray diffraction (XRD). Powder XRD analyses were performed on the dried and reduced-passivated catalyst precursors to identify the phases present in the precursor samples at various stages of synthesis. **Figure 8** shows the XRD diffractograms obtained for dried and reduced-passivated precursor samples.

The diffractogram of the diatomite support (**Figure 8a**, curve 1) shows reflections characteristic of amorphous silica (silica halo peak centered at two-theta around 21°) and the well-crystallized quartz (Q) phase (two-theta = 26.6°; JCPDS 46-1045). Typical diffractograms of dried precursor samples exhibited only broad and asymmetrical bands attributable to ill-defined and badly crystallized nickel hydrosilicates (**Figure 8a**, curves 2–6). Besides, the XRD patterns of bulk BNC disappear in the patterns of precursors. The observed phenomenon proves that an interaction occurs between BNC and silica from the support. The formation of surface lamellar hydrosilicates in the preparation of silica supported nickel catalysts was postulated on the basis of several techniques of characterization (IR, TPR, XPS and Extended X-ray Absorption Fine Structure-EXAFS). X-ray diffraction was also employed to corroborate the presence of nickel hydrosilicate. The XRD studies showed that the nickel hydrosilicates are formed under various conditions at relatively low temperatures (under 100°C) [48, 71, 78–81]. As it is well known, when the nickel salt is precipitated with Na_2CO_3 in the presence of silica, the precipitated Ni^{2+} phase is silica supported-BNC with composition of $Ni(OH)_x(CO_3)_y/SiO_2{\times}zH_2O$ that varies considerably with the changes in the precipitation conditions [41]. This interaction leads to the formation of badly ill-crystallized layered nickel hydrosilicate compounds, identified as nepouite-like (1:1 nickel hydrosilicate; $Ni_3(OH)_4(Si_2O_5)$) and/or talc-like structure (2:1 nickel hydrosilicate; $Ni_3(OH)_2(Si_2O_5)_2$). The formed phases have been identified as nickel antigorite [48, 71, 78, 81], nickel chrysotiles [82], nickel montomorillonite [48, 71], nickel palygorskite [54], serpentine [83], or orthosilicate-type [54].

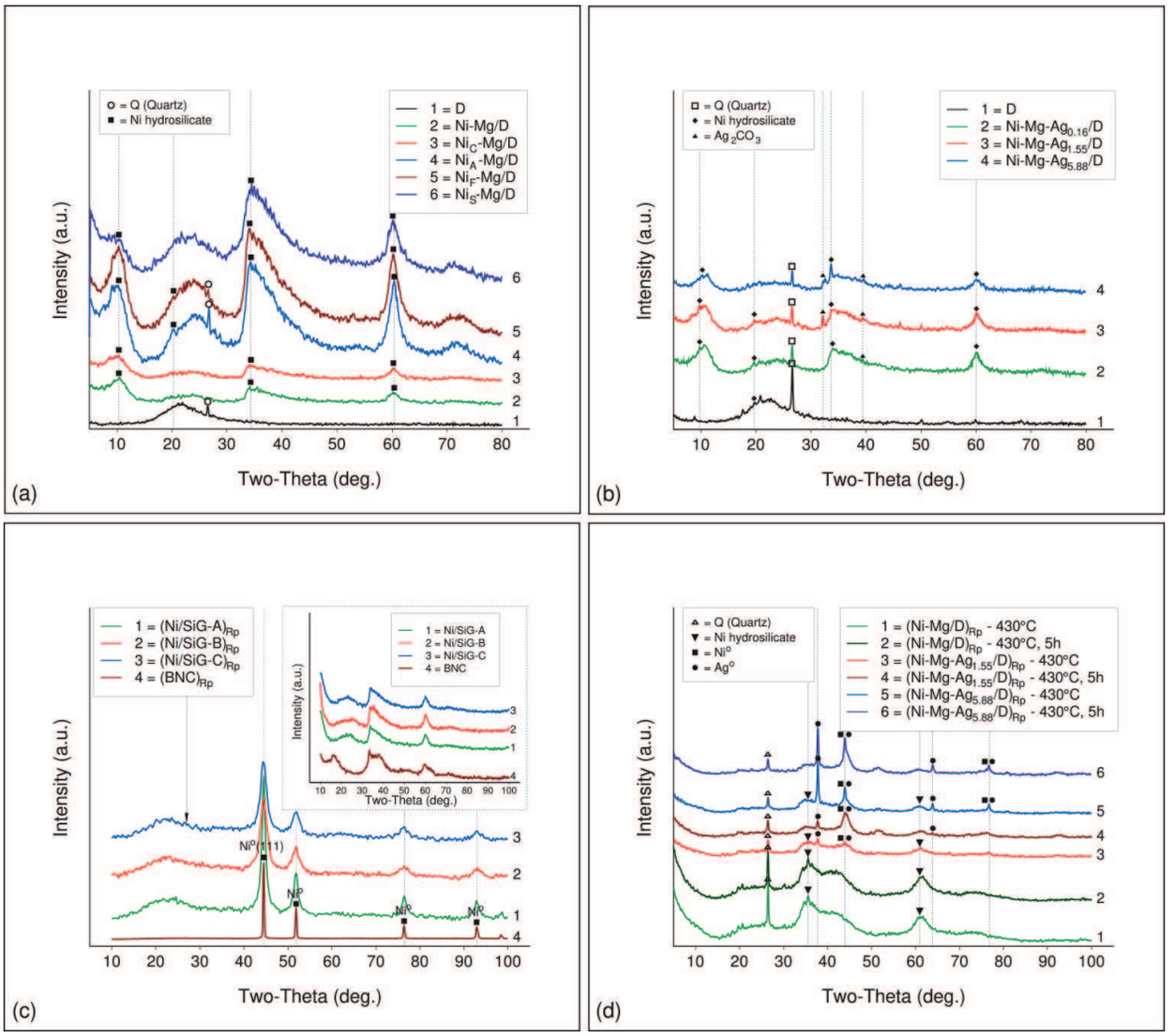

Figure 8. XRD diffractograms of supports, dried and reduced-passivated precursor samples: (a) D, Ni-Mg/D; (b) Ni-Mg-Ag/D; (c) Ni/SiG, $(Ni/SiG)_{Rp}$; (d) $(Ni\text{-}Mg/D)_{Rp}$, $(Ni\text{-}Mg\text{-}Ag/D)_{Rp}$.

Samples modified with silver (Ni-Mg-Ag/D, **Figure 8b**) have slightly altered XRD spectra. In addition to XRD peaks characteristic to the nickel hydrosilicates, two new peaks can be observed at 32.2 and 39.4° attributable to the α-Ag_2CO_3 phase (JCPDS file 31-1237). Moreover, it is observed that the modification with silver contributes to the further amorphization of the dried precursor samples [84].

The XRD patterns of the dried and reduced-passivated silica gel supported Ni catalyst precursors and reference material-BNC are presented in **Figure 8c**. The XRD patterns of three types of silica gel supports had characteristic reflections of amorphous silica (not shown). The insert in **Figure 8c** represents a comparison between the XRD patterns of the dried precursors of the Ni/SiG system and the reference BNC material. The absence of the diffraction line at 16.3° of the reference material-BNC sample and appearance of a new broad reflection at around 23° in the spectra of this catalyst precursor system represented a substantial difference between the bulk reference material and the supported Ni^{2+} phase, present in the samples of this catalyst

http://dx.doi.org/10.5772/66967

precursor system. The turbostratic structure of nickel hydrosilicate [48, 54] predetermined the ill-organized reflections of the Ni/SiG system of the precursor. Moreover, the nickel hydrosilicate phase exhibits different degrees of crystallization, more pronounced in the Ni/SIG-B sample. It is obvious that the usage of different silica gel types affects the crystallinity of the deposited Ni containing phase. Note that, the registered high background below two-theta values of 15° in XRD diffractograms of all samples indicates advanced amorphization of the observed phase.

The XRD patterns of the reduced precursor samples at 430°C (**Figure 8c**) display reflections located at two-theta, typical for nickel metal (Ni^0) (JCPDS file 00-004-0850). The peaks of lower intensity between two-theta from 32 to 40° indicate the presence of nickel hydrosilicate in all reduced samples, but it is better represented in the sample Ni/SiG-B.

In the case of the reduced catalyst precursors of $(Ni\text{-}Mg/D)_{Rp}$ and $(Ni\text{-}Mg\text{-}Ag/D)_{Rp}$ systems, typical XRD spectra showed common peaks corresponding to nickel metal (Ni^0) and silver metal (Ag^0) (**Figure 8d**). The layered structure of the nickel hydrosilicate phase was also registered. The experimental conditions for the reduction step was selected in order to establish the relation between the reduction time and the reduction temperature (selected temperature of 430°C) was assumed to be very important. Despite the obvious reduction in intensity of peaks caused by prolonged dwell time (5h) in the selected temperature, reflections corresponding to nickel hydrosilicates are still visible. This shows that the reduction temperature of 430°C used for reduction of the dried precursor with H_2 was not sufficient to reduce all the nickel hydrosilicate species to the nickel metal (Ni^0) and silica for these two systems of catalyst precursors.

The results concerning the influence of the preparation stage and nature of the support and the modifier clearly illustrate the feature of the supported Ni^{2+} phase and demonstrate that XRD measurements may offer an effective tool to identify the nickel species and their interaction with the support in differently supported and modified nickel-based catalyst precursors.

Hydrogen temperature programmed reduction (H_2-TPR). The objective of H_2-TPR experiments was to determine the reducibility as well as the optimum reduction temperature for prepared catalyst precursor systems. In conjunction with IR and XRD data, TPR profiles were also useful in determining the type of Ni^{2+} phases present in the catalyst precursors and may be indicative of the actual activity of the final reduced metal catalyst. The H_2-TPR profiles of all prepared catalyst precursors are given in **Figure 9**.

The influence of the nature of precursor salts of nickel on the reducibility of prepared samples is reported in **Figure 9a**. These results demonstrate rather well the differences between the Ni^{2+} species formed in the case of diatomite supported nickel-based catalyst precursors. A peak due to the reduction of the Ni^{2+} phase, which corresponds to the BNC (**Figure 9b–d**—insert) was seen only in the sample prepared from the sulfamate salt of nickel (Ni_S-Mg/D). Among the prepared catalyst precursors, the smallest proportion of the Ni^{2+} phase from BNC can be seen in the Ni_A-Mg/D sample. The high reduction temperature needed for the samples prepared from the acetate nickel precursor salt is obtained by the presence of difficult to reduce nickel hydrosilicates, which is the form in which nickel precipitates are deposited during synthesis. Consequently, layered nickel hydrosilicates whose thermal decomposition starts above 450°C

[47] appear to be the main nickel species present in this sample. The stronger interaction of nickel and diatomite support hinders reduction of samples. This leads to a shift in the T_{max} value of peaks corresponding to the reduction of Ni^{2+} phases interacting with the support from 320°C over Ni_S-Mg/D to 462°C over Ni_A-Mg/D. The reduction extent (R, %) of the Ni^{2+} supported phase at 430°C (**Figure 9a**) increases with the following sequence: Ni_A-Mg/D (24.8%) < Ni_F-Mg/D (26.4%) < Ni-Mg/D (43.1%) < Ni_C-Mg/D (54.5%) < Ni_S-Mg/D (75.8%).

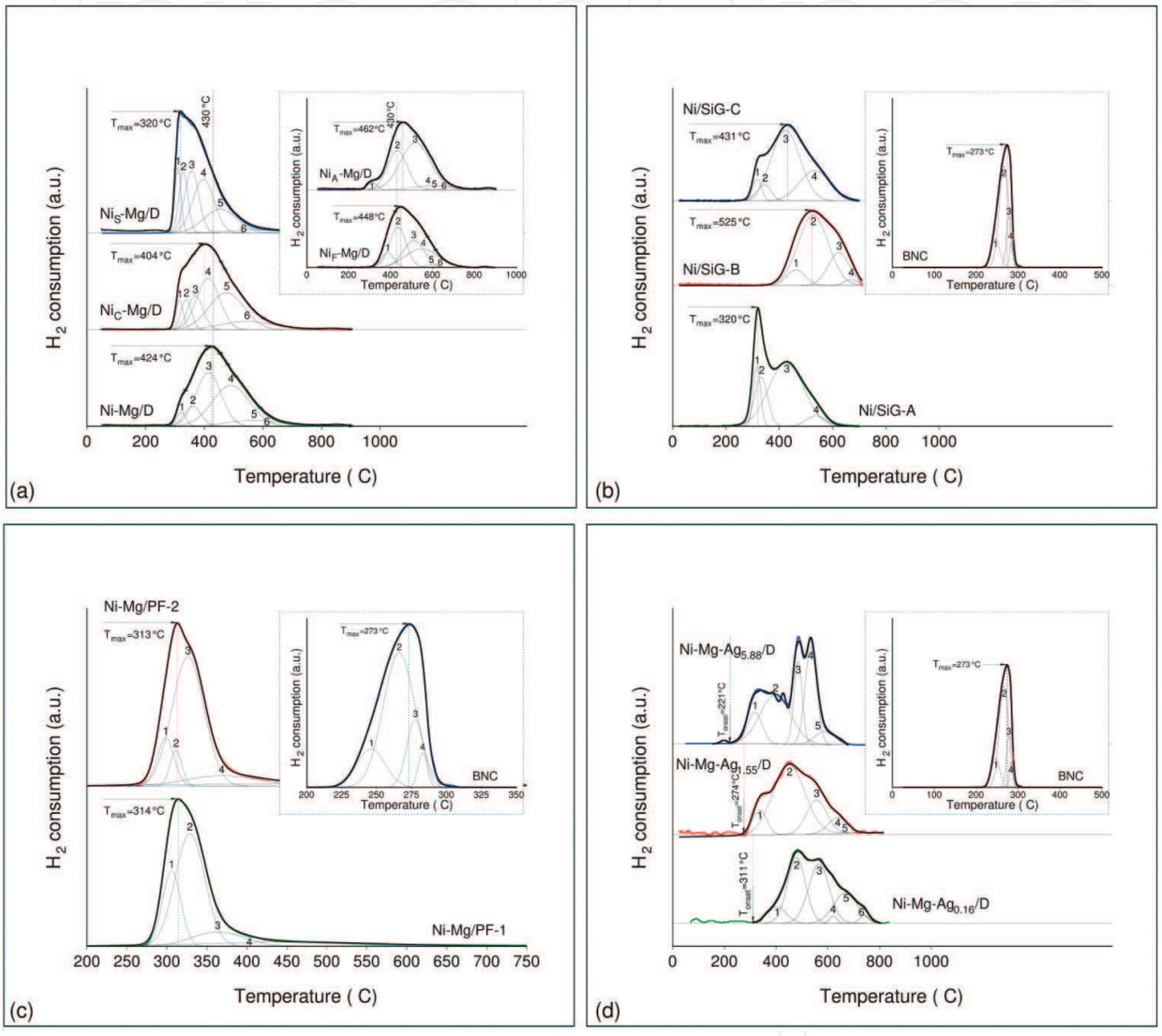

Figure 9. TPR profiles normalized to the sample weight and fitted with Gaussian deconvolution peaks for all prepared catalyst precursor systems: (a) Ni-Mg/D; (b) Ni/SiG; (c) Ni-Mg/PF; (d) Ni-Mg-Ag/D.

The reduction properties of Ni containing SiG-A, SiG-B and SiG-C catalyst precursors are shown in **Figure 9b**. The interpretation of the TPR profiles of the precursor samples is accomplished by comparing them with the profile of the reference BNC sample. The comparison is supposed to clarify the support role in the studied solids. Indeed, the experiments revealed a quite different reduction behavior of the formed Ni^{2+} species. The higher reducibility of the unsupported BNC is attested by the single low temperature peak in the region 220–310°C

which is assumed to represent the full reduction of bulk Ni^{2+} ions to the nickel metal. In contrast, multiple reduction peaks with poorly resolved maxima characterize the TPR profiles of the precursors indicating a complex interaction between the Ni^{2+} species and SiG supports. Two most distinguishable peaks at 320 and 428°C can be observed in the Ni/SiG-A sample, alongside a shoulder at 540°C. The reduction peak at 320°C can be attributed to the reduction of BNC species on Ni/SiG-A. All the reduction temperatures above this temperature can be directly associated with the different type of interaction between the nickel species and the supported material. The existence of a broader peak at 428°C and the shoulder at 540°C is caused by the strong interaction between the Ni^{2+} supported phase and the SiG-A framework which points to the existence of hydrosilicate species. The TPR profile of the Ni/SiG-C sample resembles that of the Ni/SiG-A sample with a clearly observed difference in the contribution from low temperature (BNC) and high temperature Ni^{2+} hydrosilicate species. Finally, the absence peak at 320°C and no reduction at all up to 350°C in Ni/SiG-B sample shows that BNC species does not exist, while three peaks at around 462, 525 and 624°C can be attributed to Ni^{2+} hydrosilicate species [85]. It may be summarized that the TPR profiles of the Ni/SiG system evidenced a variety of interaction strength depending on the type of the SiG support resulting in the formation of varying amounts of different Ni^{2+} species.

Reducibility of the Ni-Mg/PF precursors studied by TPR is shown in **Figure 9c**. Clearly, the profiles show almost the same tendency, since both precursors have almost the same T_{max} and slightly anti-symmetric profile toward higher temperature. The low temperature reduction at 313 and/or 314°C for Ni-Mg/PF-2 and Ni-Mg/PF-1, respectively implies the presence of bulk Ni^{2+} easily reduced species and the weak interaction between nickel and perlite support. By comparing TPR profiles of precursors with reference material (**Figure 9c**—insert) the shifting of the T_{max} of about 40°C towards higher temperatures is apparent. A reasonable postulation for a lower temperature reduction of the Ni-Mg/PF system is that it contains the majority of Ni^{2+} species nucleated as BNC and anchored to the oxygen containing groups of the perlite support after deposition. Clearly, reduction of BNC proceeds easily. Based on the entire temperature range, it can be stated that all Ni^{2+} species in this system are reducible under 430°C since no temperature profiles above this temperature have been observed. A complete reduction of the Ni^{2+} species does not necessarily mean that the catalyst will be active, due to the possibility of nickel crystallite growth through aggregation which therefore decreases the number of active sites on the support, resulting in overall decrease of catalyst activity.

The influence of the silver modifier on the reducibility of Ni-Mg-Ag/D catalyst precursors is displayed in **Figure 9d**. TPR measurements clearly showed the differences in reducibility of Ni-Mg-Ag/D samples. The TPR profile of the sample Ni-Mg-$Ag_{5.88}$/D displays five peaks. It is obvious that there are two different areas where hydrogen is consumed. The first is the low temperature region (LTR) between 210 and 440°C (TPR peaks maxima at 318 and 398°C) and the second is high temperature region (HTR) from 440 to 700°C (TPR peaks maxima at 485, 535 and 591°C). In the LTR area, the reduction of easily reducible silver (Ag^{+}) and nickel (Ni^{2+}) phases occurs. The higher TPR peak at LTR is in agreement with XRD, which also revealed the presence of more bulk-like silver upon increasing Ag loading (**Figure 8d**). Hydrogen consumption at HTR is normally attributed to hardly reducible Ni^{2+} phases—nickel hydrosilicates. When the Ag loading is decreased, the reduction profiles become less

resolved (Ni-Mg-$Ag_{1.55}$/D and Ni-Mg-$Ag_{0.16}$/D) suggesting that the reduction occurs in a single unresolved step. Obviously, increasing Ag loading in the precursors shifts the onset temperatures of the initial reduction to lower temperatures (**Figure 9d**). In addition, the reduction was completed at lower temperatures with the precursors of higher Ag loading.

Although the nickel particles of samples do not easily sinter because of the strong interaction with support [49, 72, 73], XRD and H_2-chemisorption result (discussed later in the paper) have shown that the silver loading has an impact on the reduction ability of modified catalyst precursors. The increase in the silver content leads to larger nickel particles in the Ag modified catalyst precursors, Ni-Mg-Ag/D, which displayed easier nickel reduction. In the literature, it is widely accepted as influence of reduction ability of supported metal catalysts on the particle size of the active metal: the lower the reduction ability, the smaller the nickel metal particles [56, 86]. Such a conclusion could be an explanation for better reduction ability of the catalyst precursors with higher Ag loadings.

TPR is a favorable technique for studying the impact of co-metal modifier and support effects on the ability of the reduction of supported metal catalysts [87]. The effect of adding silver on the ability of transition metals reduction is not sufficiently studied in the literature. Richardson and co-workers [88] showed the positive role of silver oxide to promote a better understanding of nickel oxide reduction. A higher degree of nickel oxide reduction in the presence of silver was interpreted by easier nucleation of the nickel clusters, which is rate determining for the reduction, according to Coenen [89]. In bimetallic silver-based catalysts, the higher the Ag loading, the deeper the reduction occurs. In the system with nickel, reduced silver forms metal particles that act as foreign nuclei for subsequent growth and reduction of nickel crystallites. The more silver cations (Ag^+) were introduced in the catalyst, the more silver nuclei formed for Ni crystallites growth and more nickel was reduced.

The TPR results demonstrate rather well the differences between Ni compound formed in the case of diatomite, silica gel and perlite. In the case of the Ni-Mg/PF system, the sharp peak at about 310°C has been identified as being due to the reduction of bulk Ni^{2+} species. The Ni-Mg/D and Ni/SiG systems are difficult to reduce and are comparable in reduction characteristics to Ni hydrosilicates. Significantly however for the Ni-Mg-Ag/D system, reduction is much more facile due to easier nucleation of the nickel crystallites in the presence of silver. In addition, it has been shown that the nature of the nickel precursor salt has a profound effect on the reducibility of Ni-Mg/D catalyst precursors.

Hydrogen chemisorption (H_2-chemisorption). Conventional supported metal catalysts are prepared by *in situ* reduction of a metal salt. The metallic surface is formed by particles of ultimate size and the rates of structure-dependent reactions depend on the size of these particles. Therefore, the catalytic activity of metal particles formed is strongly related to their size and shape. Previous work of our group showed that supported nickel nanoparticles can be obtained in the Ni/Diatomite and Ni/Water glass catalyst systems synthesized by the DP method [90]. They were found as active catalysts in partial hydrogenation of soybean oil. As to the silica support, it is known not to give rise of nickel precipitates in different oxidation states and allows a better approach of the particle size effect in the behavior of supported nickel catalysts [91].

http://dx.doi.org/10.5772/66967

The chemisorption of a gas on a catalyst surface, such as hydrogen chemisorption, is commonly used as a suitable method for the determination of the size of active metal surface area in supported metal catalytic systems [92]. The active metal surface may be measured under suitable conditions taking into account the peculiarity of the system being tested. Hydrogen chemisorption method consists of the use of a hydrogen molecule, which chemisorbs selectively on the metal and not on the support. Assuming a given stoichiometry for this surface reaction, it is possible to obtain an estimate of the metal surface area and of the average metal particle size. Thus, in the H_2-chemisorption studies, the measured value of the active metal surface is dependent on the stoichiometry of the hydrogen adsorption, which in turn depends on the metal-support interaction, modifiers and preparation method [93]. The estimation of the metal crystallite size from hydrogen uptake requires the assumptions to be made regarding metal crystallite morphology. However, it should be noted that the results of chemisorption for supported Ni catalysts in the literature are not always in agreement, mainly for two reasons: the first is that adsorption of H_2 on supported nickel catalysts involves simultaneous physical adsorption, chemisorption, reduction of Ni compound, activated adsorption and hydrogen spillover; the second is the existence of several forms of chemisorbed hydrogen bonded to surface, subsurface, edge and vertex Ni atoms.

Hydrogen chemisorption results for nickel dispersion, nickel surface area and nickel crystallite size are summarized in **Table 6**.

Although some discussion concerning the adequacy of this procedure can be found in the literature [55, 71, 92–95], the values thus obtained are useful from a comparative point of view. **Table 6** shows that a broad range of crystallite sizes is obtained as a consequence of the nickel salt precursors and modifiers used, metal loading and support type in each case. By using both static and dynamic methods under selected conditions of TPR and H_2-chemisorption experiments, the overall dispersion degree does not exceed 13% and crystallite size is lower than 23 nm (excepting the sample Ni/SiG-A). It is known that for the nickel loadings higher than 30 wt% Ni, an important decrease in dispersion is observed [55]. This fact is due to that higher nickel loadings favor agglomeration of particles. Moreover, this agglomeration process is also favored by the weak interaction between the metal and the surface of the support. Hydrogen chemisorption results showed that the particle sizes of nickel metal (Ni^0) in the samples from the different precursors salts may be correlated with their reducibility (see **Table 6** and **Figure 9a**) and textural properties (**Table 4**).

The addition of Ag (hydrogen does not chemisorb onto silver) to the Ni-Mg/D system decreased its chemisorption capacity. The cause of decreased hydrogen adsorption can be a result of blocking of the nickel active site by silver atoms, electronic interactions between Ni and Ag atoms that affect the hydrogen binding to the surface Ni and changes in the stoichiometry of hydrogen adsorption on Ni surfaces due to structure sensitivity [94]. The estimates of the crystallite size from hydrogen chemisorption are also compared with the values determined from X-ray diffraction methods line broadening (**Table 6**). The mean size of nickel particle deduced by the static H_2-chemisorption method was confirmed by the XRD method. The fact that the ratio of these two values is close to unity may be taken as added support for the assumed geometric model. The hydrogen chemisorption results for the samples of the Ni-SiG system are in agreement with their

NP measurements (**Tables 1** and **4**). The lowest dispersion of Ni/SiG-A samples is most likely caused by steric hindrances (microporous SiG-A support). In such a case, metal distribution on the external surface of the support is to be preferred, with consequent lower dispersion (the nickel content being almost the same in each sample (Ni/SiG-A, Ni/SiG-B and/or Ni/SiG-C, **Table 6**).

Sample code	Ni (wt%)	Nickel metal properties (Ni^0)				
		$H_{2\text{-chs}}$[b] ($\mu mol\ g_{Ni}^{-1}$)	S_{Ni}[c] ($m^2\ g_{Ni}^{-1}$)	$d_{Ni\ chs}$[d] (nm)	$Ni_{surf} \times 10^{-20}$ g ($at_{Ni\ acc}\ g_{Ni}^{-1}$)	D[h] (%)
Ni-Mg/D[i]	36.3	744	58.2	7.7 (7.1[e])	9.0	8.7
Ni-Mg-$Ag_{0.16}$/D[i]	35.9	709	55.5	8.1 (8.3[e])	8.5	8.3
Ni-Mg-$Ag_{1.55}$/D[i]	35.2	538	42.1	10.7 (11.7[e])	6.5	6.3
Ni-Mg-$Ag_{5.88}$/D[i]	33.5	513	40.2	11.2 (13.6[e])	6.2	6.0
Ni/SiG-A[i]	43.7	123	9.6	46.7	1.5	1.4
Ni/SiG-B[i]	45.5	571	44.8	10.0	6.9	6.7
Ni/SiG-C[i]	43.5	1073	84.0	5.3	12.9	12.6
Ni-Mg/PF-1[i]	30.2	576	45.1	9.9 (14.9[f])	6.9	6.8
Ni_A-Mg/D[j]	36.6	259	20.3	22.2	3.1	3.0
Ni_C-Mg/D[j]	36.2	437	34.2	13.1	5.3	5.1
Ni_F-Mg/D[j]	36.6	244	19.1	23.6	2.9	2.9
Ni_S-Mg/D[j]	35.0	462	36.2	12.4	5.6	5.4

[a]Each entry represents a different run.

[b]Hydrogen chemisorbed.

[c]Ni metal surface area; S_{Ni} was calculated assuming $Ni_{surf}/H_{chs} = 1$ and mean surface area of Ni atom equal to 6.5×10^{-20} m^2.

[d]Mean Ni particle or crystallite size: $d_{Ni\ chs}$ — H_2-chemisorption method (surface mean value).

[e]Mean Ni particle or crystallite size: $d_{Ni\ XRD}$ – XRD line broadening method (volume mean value); Ni crystallite geometric model: hemispherical crystallites attached to support with their equatorial plane.

[f]Computed assuming spherical model.

[g]Number of accessible Ni atoms-exposed fraction.

[h]Dispersion.

[i] Chemisorption method: static.

[j]Chemisorption method: dynamic.

Table 6. Chemisorption experiments on the selected samples of Ni-Mg-Ag/D, Ni/SiG and Ni-Mg/PF systems[a].

Comparison was made between Ni-Mg/PF-1 and Ni-Mg/D samples. A smaller metal surface area and a larger Ni crystallite size can be observed in Ni-Mg/PF-1 and attributed to the rapid aggregation of nickel crystallites formed in the reduction stage. It is likely that the reason for this behavior is the weak interaction between the PF support and the Ni surface. For this sample, a crystallite size of nickel calculated assuming a spherical model which is suitable for the supported catalysts with weak metal-support interaction represents a more realistic result (**Table 6**). On the contrary, a larger nickel metal surface area and a smaller nickel particle size is observed on the Ni-Mg/D sample due to the strong anchoring effect of D support.

This anchoring restricts the migration of nickel particles hence prevents the formation of large nickel particles that did not sinter on the mild reduction at 430°C.

The hydrogen chemisorption study showed that the size of nickel nanoparticles obtained in the studied catalyst precursor systems depended on the nature of precursor nickel salt from which they are formed, the kind and loading of metal modifier and the type of support used.

X-ray photoelectron spectroscopy (XPS). In the previous part of this work, it was pointed out that two major factors that affect the reduction of Ni^{2+} supported phase are: (i) interaction between precipitating nickel precursors and the catalyst support and (ii) the dispersion nickel metal phase (Ni^0) arising by reduction of the deposited Ni^{2+} phase. These factors are in turn affected by various examined parameters including the nature of the support, the use of modifier and the choice of nickel precursor salt. Useful confirmatory evidence concerning the interaction between the Ni^{2+} supported phase and support including the structural changes occurring during preparation, drying and reduction and the dispersion of nickel metal phase can be obtained by photoelectron spectroscopy. XPS is virtually surface sensitive (a few atomic layers) and a quantitative instrumental method particularly suitable for the evaluation of surface character of supported nickel catalysts [96].

The XPS results discussed in this work will be restricted to the cases of Ni/SiG, Ni-Mg/D and Ni-Mg-Ag/D systems. The XPS spectra of the Ni 2p and Ag 3d peaks for the systems under investigation are shown in **Figure 10**.

On investigating the influence of the support characteristics on the strength of the interaction between Ni containing species and the support, we chose the Ni/SiG precursor system keeping in mind that the interaction between the Ni^{2+} species and the support is commonly accepted depending on the characteristics of the support. By choosing such a system containing the samples prepared without addition of the modifier with almost the same Ni loadings (**Table 3**), we hoped to increase the value of any comparison one may make. The 2p peaks in the nickel spectrum were used to characterize the chemical state of nickel. The intensity of the Ni 2p signal was obtained by integration over the binding energy (BE) range of 850–890 eV to include the double excitation, shake-up and shake-off peaks. It is known that the chemical forms of nickel have certain characteristics, which serve to identify their presence [97]. The shape of the peaks also contains information. The separation and intensity of the shake-up satellite of the Ni $2p_{3/2}$ core level can be helpful in identifying a particular species.

As expected for dried samples, nickel in these precursors is present in the Ni^{2+} oxidation state—Ni $2p_{3/2}$ peak is a doublet structure (splitting a few electronvolts). The nickel 2p core level, as seen in **Figure 10a**, is similar in shape for all samples, however, the binding energies of the Ni 2p level vary from each other. Since XPS is surface sensitive, the differences in binding energies of the XPS peaks indicate that the nickel species on the surface are changed. The XPS data in **Table 7** show that the binding energies of the Ni $2p_{3/2}$ level for the Ni/SiG-A sample and for the reference material (BNC) are the same. It means that the aggregates of BNC are situated on the surface of nickel hydrosilicates located on the precursor SiG-A [72, 98]. The chemical shift of the Ni $2p_{3/2}$ peak toward higher binding energy values

for the Ni/SiG-B sample is assigned to the stronger interaction between the Ni^{2+} species and the SiG-B support. On the contrary, the observed shift toward lower binding energies for the Ni-SiG-C sample suggests weakening interaction between the Ni^{2+} supported phase and the SiG-C support [68]. **Table 7** reveals the variations of the Ni/Si ratio suggesting the different dispersion of the Ni^{2+} species in analyzed samples, as previously shown in the H_2-chemisorption results of the corresponding precursor samples (see **Table 6**).

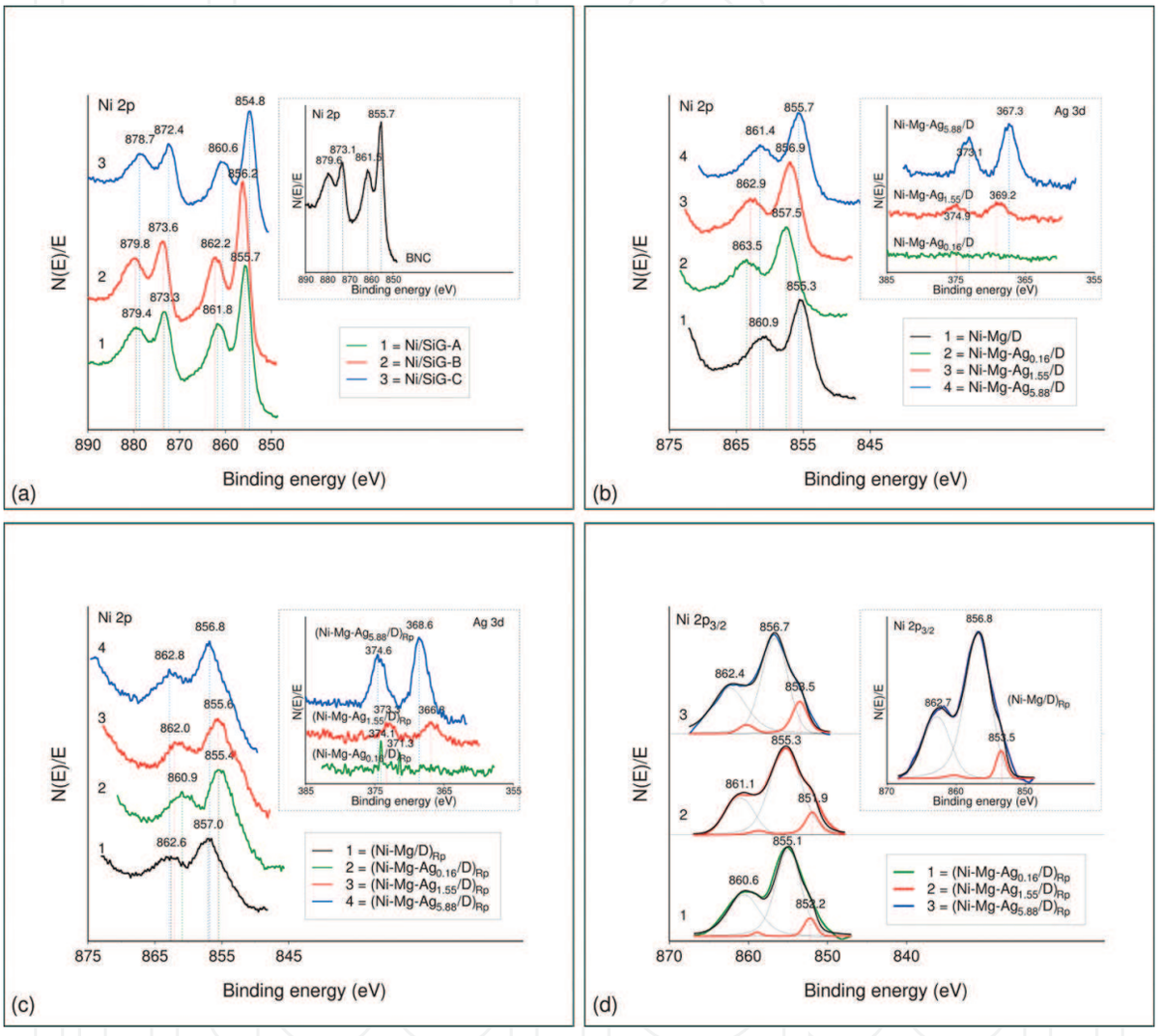

Figure 10. Ni $2p_{3/2}$ XPS spectra of supported nickel catalyst precursors: (a) dried Ni/SiG; (b) dried Ni-Mg/D, Ni-Mg-Ag/D; (c) reduced passivated $(Ni\text{-}Mg/D)_{Rp}$, $(Ni\text{-}Mg\text{-}Ag/D)_{Rp}$; (d) reduced passivated $(Ni\text{-}Mg/D)_{Rp}$, $(Ni\text{-}Mg\text{-}Ag/D)_{Rp}$ (deconvoluted).

The XPS spectra for diatomite supported nickel-based catalyst precursors are presented in **Figure 10b–d**. The Ni 2p core level signal of dried Ni-Mg/D and Ni-Mg-Ag/D precursor samples consist of a single Ni $2p_{3/2}$ peak centered at around 855 eV (Ni-Mg/D and Ni-Mg-$Ag_{5.88}$/D) assigned to Ni^{2+} (**Figure 10b**). The existence of a second component at a higher BE (860.9-863.5) could be due to the presence of hardly reducible Ni^{2+} species, as previously noted in the discussion of the corresponding TPR curves. Ag 3d XPS spectra for dried Ni-Mg-Ag/D catalyst precursors are depicted in **Figure 10b**—insert. There are two peaks, a

result of spin-orbit splitting, designated Ag $3d_{5/2}$ and Ag $3d_{3/2}$, respectively, corresponding to the strongest photoelectron lines. These peaks are observed at 367.3 eV and 373.1 eV, respectively, shifted to lower BE values in relation to metallic Ag and could be assigned to the Ag^{+} oxidation state [99]. Silver modification provokes a shifting of the Ni $2p_{3/2}$ peak toward higher BE values. The observed shift could be due to the interaction between the components in the dried samples, which is more intense for the sample with the lowest Ag loading.

Sample code	Binding energy (eV)	Surface concentration (at%)			Surface atomic ratio
		Ni	O	Si	Ni/Si
Ni/SiG-A	855.7	21.1	64.6	13.9	1.5
Ni/SiG-B	856.2	14.2	67.4	17.9	0.8
Ni/SiG-C	854.8	15.0	70.6	14.3	1.1
BNC	855.7	27.7	72.3	–	–

Table 7. X-ray photoelectron spectroscopy data for Ni-SiG catalyst precursors—dried samples.

After H_2 reduction, a shoulder appears on the low binding energy side of the Ni $2p_{3/2}$ peak (**Figure 10d**). The shoulder can be deconvoluted and the binding energy is that of the nickel metal (851.9 eV). The other peaks observed on the reduced-passivated samples at higher BE values assigned to Ni^{2+} also appear. The presence of Ni^{2+} species after H_2 reduction has also been confirmed by IR and XRD (**Figures 7d** and **8d**). It is worth mentioning that the increase of Ag $3d_{5/2}$ binding energy after reduction treatment with the respect to the dried precursors (**Figure 10c** and **b**—insert). Although it is known that silver oxides are quite unstable and the two silver oxides, Ag_2O and AgO, decompose below the temperature of 230°C, even in the oxygen atmosphere [100, 101] the results of the Ag 3d and O 1s (not shown here) XPS spectra seem to suggest the presence of silver (I) oxide on the surface of reduced-passivated samples.

The XPS study of Ni/SiG, Ni-Mg/D and Ni-Mg-Ag/D precursor samples confirm the formation of surface species with different strength of interaction and different dispersion of the supported nickel species.

3.2. Partial hydrogenation of soybean oil (SBO)

3.2.1. Activity of Ni-Mg/D and Ni-Mg-Ag catalysts in partial hydrogenation of SBO

Hydrogenation overall activity was monitored by the decay of the iodine value which indicates the level of unsaturation of double bonds (C=C). Activity (A) was calculated from the following equation:

$$A = \frac{H_{2c}}{t \cdot m_{oil} \cdot Ni_{lcc}} \quad (1)$$

where H_{2c} is the hydrogen consumption for decay in iodine value; t is the reaction time; m_{oil} is mass of oil; and Ni_{lcc} is the nickel loading in the catalyst charge for hydrogenation run (in grams).

The results of SBO hydrogenation over Ni-Mg/D and Ni-Mg-Ag/D catalysts in the slurry pilot-plant reactor system (**Figure 4**) are presented in **Table 8**.

Sample code	Activity results[a]					
	Ni_{lcc} [b] (g)	IV_{final} [c]	t (min)	H_{2c} [d] (mol)	r_{H2c} [e] (μmol H_2 min^{-1} g_{oil}^{-1})	A (μmol H_2 min^{-1} g_{Ni}^{-1} g_{oil}^{-1})
Ni-Mg/D	0.9972	89.3	75	8.018	21.3	21.4
Ni-Mg-$Ag_{0.16}$/D	0.8985	90.6	81	7.762	19.2	21.3
Ni-Mg-$Ag_{1.55}$/D	0.8790	90.0	155	7.880	10.2	11.6
Ni-Mg-$Ag_{5.88}$/D	0.8377	90.0	255	7.880	6.2	7.4

[a]Process parameters: 160°C (temperature); 0.16 MPa (H_2 pressure); 750 rpm (stirring rate).
[b]Ni loading in catalyst charge for hydrogenation run (catalyst concentration: 0.05 wt%, i.e., 2.5 g catalyst/5000 g oil).
[c]Iodine value determined by Wijs method.
[d]Hydrogen consumption for decrease of iodine value by *ca* 40–41 units.
[e]Rate of hydrogen consumption per unit mass of oil.

Table 8. Soybean oil hydrogenation over Ni-Mg/D and Ni-Mg-Ag/D catalysts in slurry pilot plant reactor system—catalytic activity test runs results.

The obtained results showed clearly the influence of the silver addition on the catalyst activity. Under the same process conditions, Ni-Mg/D and silver modified catalysts exhibited different activities toward SBO hydrogenation (see **Table 8**). By comparing the results of catalytic test runs over Ni-Mg/D and Ni-Mg-$Ag_{0.16}$/D catalysts, it can be observed that the activity of the sample without silver is slightly higher. The modification by silver inhibits hydrogenation activity, this effect being more obvious as the Ag loading is higher. From these results, the hydrogenation activity for the studied catalyst (**Table 8**) increases in the following order: Ni-Mg-$Ag_{5.88}$/D < Ni-Mg-$Ag_{1.55}$/D < Ni-Mg-$Ag_{0.16}$/D < Ni-Mg/D.

The observed differences in the activity of the studied catalysts could be attributed to nickel dispersion and different textural properties of the catalysts. From the chemisorption results, the silver-modified Ni catalyst sample with high loading (Ni-Mg-$Ag_{5.88}$/D) demonstrated 6.0% nickel dispersion and an average nickel crystallite size of ≈ 11 nm. A higher nickel dispersion and a smaller nickel crystallite size were obtained for the Ni-Mg/D catalyst sample (**Table 6**). Besides, among the studied catalysts Ni-Mg catalyst sample had the highest S_{BET} surface area (**Table 4**). This indicates that the role of catalyst texture and dispersion of the active phase is critical in assessing the catalytic efficiency. In considering an explanation for the diminished hydrogenation activity of silver modified nickel catalyst it can be also assumed a physical blocking of nickel active sites or even changes in the morphology of nickel metal particles by the silver modifier. It is difficult to discriminate between these different possibilities. Apart from the effect of co-metal blocking of the surface nickel atoms, it should also be noted that an

electronic effect has been taken into account [94]. It must be noted that the electronic properties of very small particles—nanoparticles should be different from those of large particles at least for two reasons. The first relates to the differences in the fraction of the total atoms that are present on the surface. The second is the incomplete coordination of the surface atoms from those in the bulk. Based on the assumption that catalytic activity of a metal is related to its electronic properties, it seems reasonable that the activity would vary with the crystallite size. However, a clearer understanding of the factors responsible for the crystallite size effects will require more information on the properties of nanoparticles.

3.2.2. Cis/trans isomerization

The factors influencing the *cis*/*trans* composition are catalyst activity and loading, as well as process conditions that include the hydrogen pressure, temperature and stirring rate. These parameters determine the hydrogen concentration on the catalyst surface, which is crucial not only for hydrogenation of double bonds but for *cis*/*trans* isomerization as well.

The hydrogenation of SBO is a complex network of chemical reactions involving consecutive saturation of C18:3*c* to C18:2*c*, C18:2*c* to C18:1*c* and subsequent saturation of C18:1*c* to C18:0 as well as parallel reversible isomerization of C18:2*c* to C18:2*t* and C18:1*c* to C18:1*t*. The overall hydrogenation reaction scheme may also involve a simple step hydrogenation of C18:1*t* to C18:0 and C18:2*t* to C18:1*t*.

The fatty acid compositions of hydrogenated SBO at conversion of 30.8 ± 0.5% are shown in **Table 9**. The experimental data of the fatty acid compositions in hydrogenated SBO summarized in **Table 9** showed that in all the cases, there was an increase in the concentration of stearic acid (C18:0). On the contrary, a decrease in linoleic acid (C18:2*c*) was also observed in all the cases. It should be noted that linolenic acid (C18:3*c*) conversion after 30 min of reaction was 100% when the hydrogenation was performed over any of the studied catalysts. Taking into account a known fact that silver modified catalysts show high saturation selectivity toward linoleic acid (C18:2*c*) [102], disappearance of linolenic acid in the early stage of the hydrogenation was an expected result. As the present work is focused on the control of the TFAs, the geometric isomers are presented in **Table 9** without taking into account the position of double bond in the fatty acid chain, only distinguishing between *cis* fatty acids (CFAs) and TFAs.

From these results, it is evident that the Ni-Mg-$Ag_{5.88}$/D catalyst formed the least TFAs of all catalysts (23%) at the same conversion level. On the contrary, the Ni-Mg/D catalyst was demonstrated to have the highest content of TFAs (62.1%), which could be associated with its activity manifested in SBO hydrogenation and a higher total surface area compared to the catalyst with a silver modifier. It is well known that a large surface area encourages the isomerization reactions, due to the greater accessibility to the nickel active sites [103]. A small increase of stearic acid in the order: Ni-Mg-$Ag_{5.88}$/D < Ni-Mg-$Ag_{1.55}$/D < Ni-Mg-$Ag_{0.16}$/D < Ni-Mg/D could be explained by the differences observed in their textural properties (**Tables 4** and **5**). According to Balakos and Hernandez [13], small pores favor fatty acid saturation, since the successive hydrogenation is made easier by the mobility difficulties of the bulky molecule. The catalytic

test results clearly show that adding silver to the Ni-Mg/D system have a considerable effect on the distribution of CFAs and TFAs in hydrogenated oil. A higher ratio of unsaturated *cis* fatty acids to *trans* fatty acids over the Ni-Mg-$Ag_{5.88}$/D catalyst can be attributed to the smaller formation of TFAs, suggesting a more selective hydrogenation reaction. The modification with silver is beneficial in limiting the C18:1 *cis*/*trans* isomerization during the SBO hydrogenation. On the other hand, the addition of silver did not have significant effect on the formation and distribution of C18:2*t* isomers (C18:2*c*,*t* + C18:2*t*,*c* + C18:2*t*,*t*), indicating that the main reason for the difference in the specific isomerization selectivity (S_i) was favored isomerization of elaidic fatty acid (C18;1*t*) over the Ni-Mg/D catalyst sample. Concerning the isomerization selectivity (S_i), the addition of silver provoked the reduction of TFAs (R_{trans}) in the range of 4–57% during SBO hydrogenation with respect to the Ni-Mg/D catalyst (see **Table 9**).

Fatty acid	**Catalyst sample**			
	Ni-Mg/D	**Ni-Mg-$Ag_{0.16}$/D**	**Ni-Mg-$Ag_{1.55}$/D**	**Ni-Mg-$Ag_{5.88}$/D**
C18:0	8.6	8.1	6.2	5.8
C18:1*c*	15.9	18.7	22.5	22.7
C18:1*t*	53.1	49.1	16.5	10.8
C18:2*cc*	0.9	1.2	22.7	31.7
C18:2*tt*	1.7	1.4	2.5	2.0
C18:2*ct*	2.9	3.9	7.6	6.9
C18:2*tc*	3.5	4.2	8.3	6.6
C18:2*t*[b]	8.1	9.5	18.4	15.5
C18:3*c*	none	none	none	none
Others[c]	13.3	13.6	13.7	13.5
CFAs/TFAs	0.3	0.3	1.3	2.1
S_i[d1]	1.5	1.5	0.9	0.6
S1[d2]	1.1	1.1	3.1	1.8
R_{trans} (%)[e]	–	4.2	43.0	57.0

[a]Conversion (%) = $[(IV_0–IV_f)/IV_0] \times 100 = 30.8 \pm 0.5$.

[b]Sum of *ct*, *tc* and *tt* fatty acid isomers.

[c]Sum of C14:0, C16:0, C16:1, C20:0, C20:1 and C22:0 fatty acids.

[d]Selectivity basically means that the reaction is guided toward a particular unsaturated bond in preference to others; [d1]Si—specific isomerization selectivity, defined as quotient of TFAs (%) in hydrogenated oil product and change in iodine value between the starting oil and hydrogenated product; [d2]S1—selectivity 1, defined as the amount of monounsaturated fatty acids (C18:1) formed with respect to the amount of diunsaturated (C18:2) converted: $S1 = (C18:1–C18:1_{(0)})/(C18:2_{(0)}–C18:2)$.

[e]R_{trans}—reduction TFAs, defined as: $R_{trans} = \{1 - [\Delta(C18:1t+C18:2t)_{catalyst2}/\Delta(C18:1t+C18:2t)_{catalyst1}]\} \times 100$, $\Delta(C18:1t+C18:2t)_{catalyst1} > \Delta(C18:1t+C18:2t)_{catalyst2}$, C18:2*t*—sum of *ct*, *tc* and *tt* fatty acid isomers.

Table 9. Soybean oil hydrogenation over Ni-Mg/D and Ni-Mg-Ag/D catalysts in slurry pilot plant reactor system—fatty acids composition[a] and selectivities[d, d1, d2].

In general, the overall hydrogenation selectivity decreased while the isomerization increased with conversion. The mechanisms of the hydrogenation and *cis*/*trans* isomerization are strongly interrelated. An addition-elimination mechanism according to Horiuti-Polanyi is often assumed to describe the formation TFAs in the hydrogenation processes [58]. The original concept of Horiuti-Polanyi mechanism provides that hydrogenation and isomerization should both be described by a half-hydrogenated state mechanism. Since hydrogenation is accompanied by isomerization, it can be proposed that the electron donor characteristics of the silver modified nickel catalyst would also affect this reaction. If the chemisorbed half-hydrogenated intermediate is removed quickly enough, it may not have time to isomerize to *trans* or in the case of linoleic acid, when hydrogenation of one of the double bonds is complete, the fatty acid molecule is released before hydrogenation of the second double bond can occur. The limited formation of C18:1*t* over silver modified Ni-Mg-Ag/D catalytic system compared to that of the Ni-Mg/D system may be explained by both, the changing of electronic properties and the presence of geometric effect. The promoting effect of adding silver to the Ni-Mg/D system for SBO hydrogenation is manifested for all the catalysts tested in this work when considering the reduced TFA formation.

3.2.3. Kinetic study of SBO hydrogenation

Several kinetics models of the hydrogenation of fatty oils containing polyunsaturated fatty acids were devised previously and reaction rate constants were evaluated for the various reactions [104–107]. All of the proposed kinetic models including various reaction pathways were incomplete. From a practical standpoint, it is justified because of the extreme complexity of the complete kinetic model, which would have to include all possible consecutive and isomerization reactions.

A mathematical model has been developed to describe the kinetics of both the hydrogenation and the *cis*/*trans* isomerization of SBO. A simple approach to model the rate constants for SBO hydrogenation over studied catalysts is presented. The rate constant model is constructed assuming the first order rate equations with respect to the compositions of the various *cis* and *trans* fatty acids in the hydrogenated SBO. In this model, the fatty acids are divided into five groups: (i) C18:2*c*—*cis* diunsaturated; (ii) C18:2*t*—*trans* diunsaturated; (iii) C18:1*c*—*cis* monounsaturated; (iv) C18:1*t*—*trans* monounsaturated; (v) C18:0—saturated (stearic acid). Mathematical equations were developed for all groups of fatty acids as a function of reaction time. The k_i's (i = 1–8) are the respective first order reaction rate constants. Numerical solutions for the set of ordinary differential equations corresponding to the kinetic model were obtained through the Gear algorithm [108]. The rate constants were computed from the kinetic experiments by minimizing the sums of squares for deviations between the computed and experimental concentrations of studying fatty acids. The minimization was performed by the simplex method [109].

A reaction scheme, time dependence concentration of fatty acids and the estimated rate constants are presented in **Figure 11** and **Table 10**.

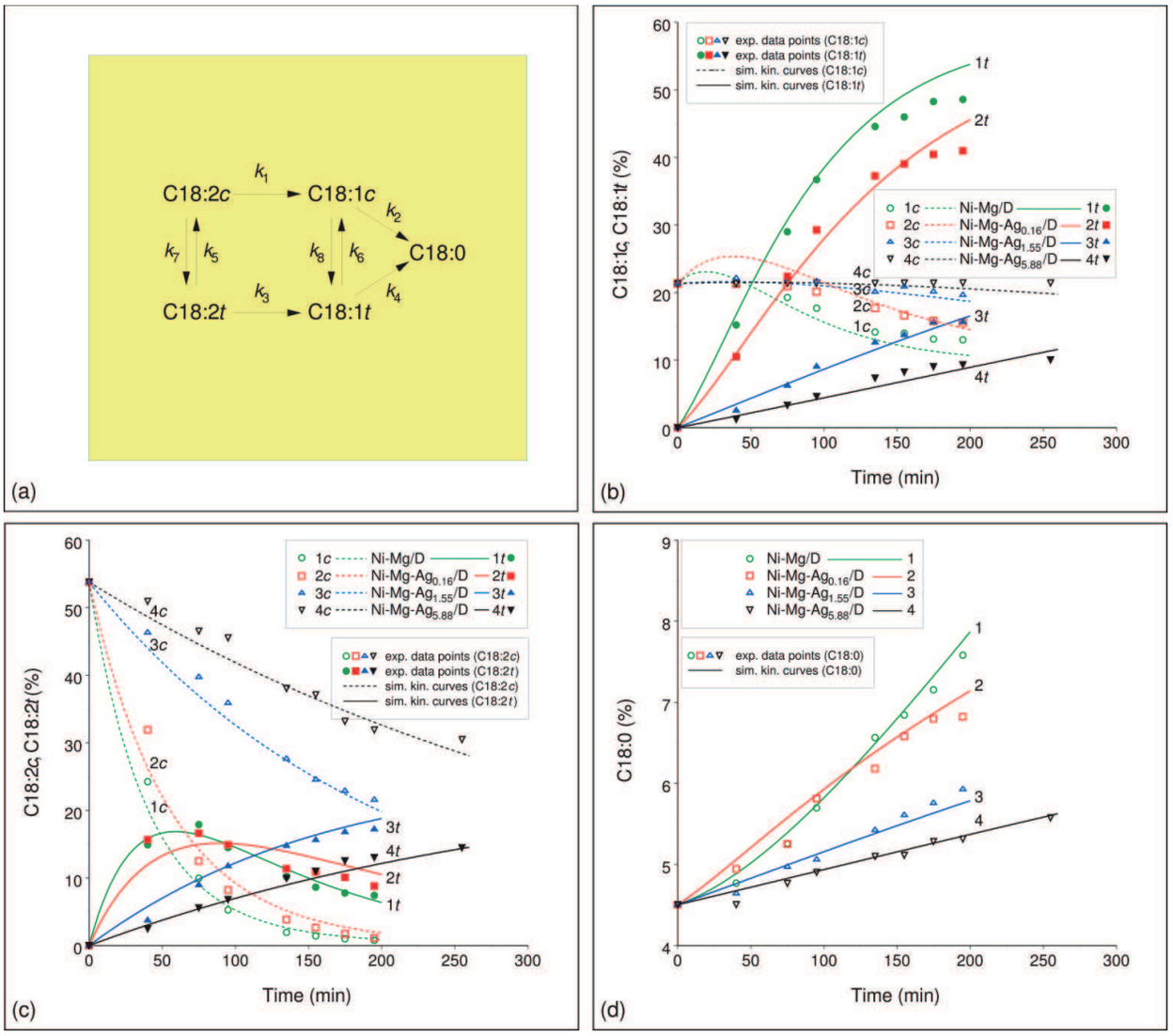

Figure 11. Hydrogenation of SBO: (a) reaction scheme; (b–d) correlation between experimental data and model predictions for SBO hydrogenation over Ni-Mg/D and Ni-Mg-Ag/D catalytic systems under operating conditions used.

Sample code	Rate constants[a]							
	k_1 (min^{-1})	k_2 (min^{-1})	k_3 (min^{-1})	k_4 (min^{-1})	k_5 (min^{-1})	k_6 (min^{-1})	k_7 (min^{-1})	k_8 (min_{-1})
Ni-Mg/D	1.0×10^{-2}	3.0×10^{-4}	1.0×10^{-2}	3.5×10^{-4}	1.5×10^{-3}	2.5×10^{-3}	1.5×10^{-2}	1.5×10^{-2}
Ni-Mg-$Ag_{0.16}$/D	0.9×10^{-2}	5.6×10^{-4}	6.0×10^{-3}	6.0×10^{-5}	6.0×10^{-4}	2.0×10^{-3}	9.0×10^{-3}	1.0×10^{-2}
Ni-Mg-$Ag_{1.55}$/D	0.2×10^{-2}	3.0×10^{-4}	0.7×10^{-3}	2.5×10^{-5}	0.1×10^{-4}	0.9×10^{-3}	3.0×10^{-3}	4.0×10^{-3}
Ni-Mg-$Ag_{5.88}$/D	0.1×10^{-2}	2.0×10^{-4}	0.4×10^{-3}	2.0×10^{-5}	0.1×10^{-4}	0.1×10^{-3}	1.5×10^{-3}	2.0×10^{-3}

[a]Refers to the first order kinetic rate constants.

Table 10. Hydrogenation of soybean oil over Ni-Mg/D and Ni-Mg-Ag/D catalysts—computed values of the rate constants (T = 160°C).

Table 10 reveals that the rate constants of isomerization reaction k_7 and k_8 and constant of saturation reaction k_4, corresponding to the stearic acid formation, are higher in the case of Ni-Mg/D and Ni-Mg-$Ag_{0.16}$/D catalyst samples. These observations are in agreement with experimental data, shown in **Table 9** related to the formed C18:1*t* and C18:0 during the hydrogenation of SBO.

Figure 11b–d shows a comparison between experimentally measured and simulated modeling kinetics curves (parity plots for C18:1*c* and C18:1*t*—**Figure 11b**; C18:2*c* and C18:2*t*—**Figure 11c**; C18:0—**Figure 11d**). As it can be seen, generally, the difference between experimental results and model estimation is within 10%, which confirms the accuracy of the results. A model agrees with the general knowledge in hydrogenation and the data were fitted fairly well by the model. The proposed kinetic model could be applicable for the hydrogenation of SBO under studied operating conditions.

3.3. Partial hydrogenation of sunflower oil (SFO)

3.3.1. Activity of Ni/SiG and Ni-Mg/PF catalysts in partial hydrogenation of SFO

The Ni/SiG and Ni-Mg/PF catalysts were tested for comparison, in order to determine their activity in the sunflower oil hydrogenation. The obtained results in the laboratory reactor system (**Figure 3**) are shown in **Table 11** and **Figure 12**.

Sample code	Activity results[a]					
	Ni_{lcc}[b] (g)	$IV_{selected}$[c]	t (min)	H_{2c}[d] (mol)	r_{H2c} (μmol H_2 min^{-1} g_{oil}^{-1})	A (μmol H_2 min^{-1} g_{Ni}^{-1} g_{oil}^{-1})
Ni/SiG-A	0.5510	108.7	18.55	0.894	53.5	97.2
Ni/SiG-B	0.5510	108.7	180.00	0.894	5.5	10.0
Ni/SiG-C	0.5511	108.7	47.34	0.894	21.0	38.1
Ni-Mg/PF-1	0.5400	108.7	6.92	0.894	143.5	265.8

[a]Process parameters: 160°C (temperature); 0.20 MPa (H_2 pressure); 1200 rpm (stirring rate).
[b]Ni loading in catalyst charge for hydrogenation run; Ni concentration: 0.06 wt% with respect to oil.
[c]Selected value of IV to compare catalyst activity corresponds to the final iodine value (IV_f) in the hydrogenation of sunflower oil over the catalyst with the lowest activity (Ni/SiG-B).
[d]Hydrogen consumption for decrease of iodine value from starting (131.5) to selected value.

Table 11. Sunflower oil hydrogenation over Ni/SiG and Ni-Mg/PF catalysts in laboratory reactor system—catalytic activity test runs results.

A comparative study of SFO hydrogenation over Ni/SiG catalyst samples was performed at the same level of conversion (17.3%) in order to obtain more accurate comparative results. Activity was calculated according to Eq. (1) as hydrogenation overall activity, referred to the hydrogen consumption for a target IV value of 108.7. Analyzing the activity presented in **Table 11**, a significant variation of the values obtained for the different catalysts can be observed. As all catalysts are expected to present the same kind of active sites (metallic nickel), an explanation

for this behavior should be sought in different structural and textural properties of the studied catalysts. Considering the structure of the Ni/SiG-A, Ni/SiG-B and Ni/SiG-C samples and dispersion of the nickel metal, no clear correlation of the experimental data was found. It is likely that nonuniform distribution of nickel is the main reason for this behavior of the studied catalysts. To verify this assumption, it is necessary to establish a functional relationship between the concentration of the available nickel surface area in the reaction mixture and the initial global hydrogenation rate [110]. Analyzing the results of NP measurements for the Ni/SiG system (**Table 4**), it appears that the activity of the samples is associated with their mesoporosity. The hydrogenation overall activity Ni/SiG-B < Ni/SiG-C < Ni/SiG-A follows the same order as surface area in the mesopore range (available for the hydrogenation, see **Tables 4** and **11**).

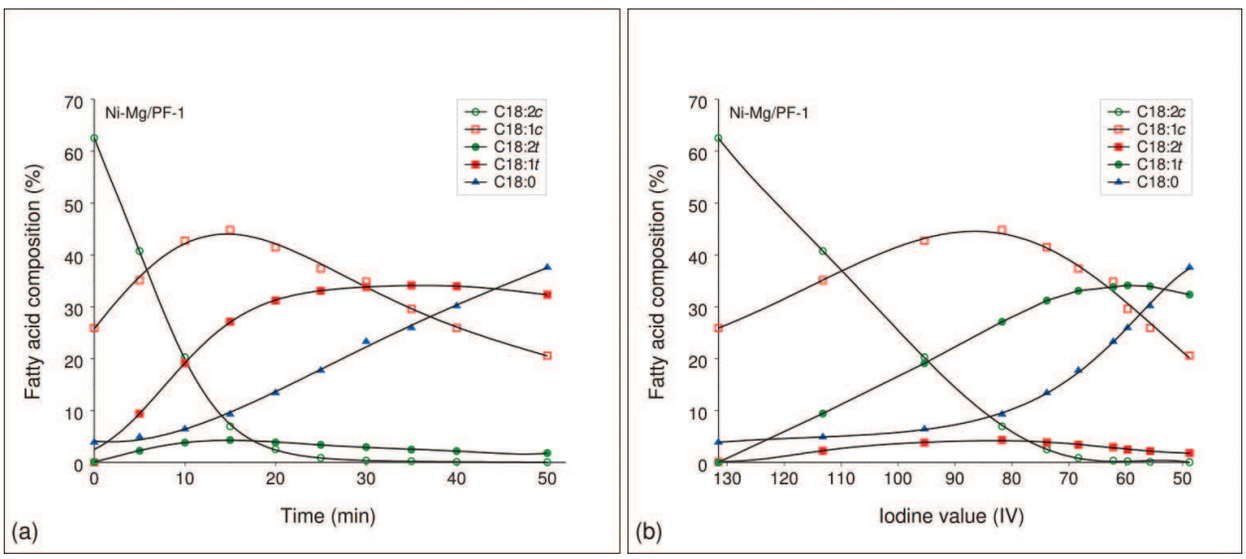

Figure 12. Time course (a) and IV decay (b) profiles of reactants and products during the hydrogenation of SFO over the Ni-Mg/PF-1 catalyst.

Regarding the performance of the Ni-Mg catalyst supported on perlite (Ni-Mg/PF-1), the hydrogenation activity was found to be very high. In addition, the Ni-Mg/PF-1 catalyst demonstrated a high activity in SFO deep hydrogenation (decrease in IV of 82.8, **Figure 12**) [31].

In **Figure 12a**, linoleic acid (C18:2*c*) was almost depleted within 30 min of reaction. This may be attributed to complex reactions evolving concomitantly. Such reactions may include hydrogenation of C18:2*c* to C18:1*t*; isomerization of C18:2*c* to C18:2*t* then hydrogenation to C18:1*t* as well as isomerization of C18:12*c* to C18:1*t*. The level of oleic acid initially increased, then leveled off; while the stearic acid rapidly increased. The monoenic *trans* fatty acid content (C18:1*t*) monotonically increased up to 33.8% after 30 min of reaction and continued to decrease slowly reaching a final level of 32.3%. Dienic *trans* fatty acid profiles (C18:12*t*) exhibited a different behavior characterized by an increase up to 4% followed by a decrease due to their conversion to stearic acid and possibly also to *trans* monoenic acid (C18:1*t*). From the standpoint of health and technical functional properties, taking into account unsatisfactory product distribution (34.3% TFAs and 37.6% stearic acid), it is necessary to optimize the properties of this catalyst with the aim of finding a good compromise between the activity and capacity to produce undesirable TFAs and stearic acid.

http://dx.doi.org/10.5772/66967

3.3.2. Kinetic study of SFO hydrogenation over Ni/SiG catalysts

A lumped kinetic model was developed to describe the evolution of the products during the SFO hydrogenation over the Ni/SiG system. This model considers the saturation of double bonds along the fatty acid chains and *cis*/*trans* isomerization, which take place simultaneously with the hydrogenation of fatty acids. The assumed reaction pathway is described in **Figure 13a**. The reaction pathway contains 12 reactions that include all possible reactions. The reaction scheme does not exclude reverse isomerization reactions (*trans* to *cis*), nor does it exclude hydrogenation with isomerization (C18:2*t* to C18:1*c*), but their low probability is emphasized with dashed arrows (see **Figure 13a**). Due to the fact that there are 12 reactions we considered all 12 reaction rate constants. For calculation of kinetic parameters, the same method as for the hydrogenation of SBO was used. Lines in **Figure 13b–d** depict the predicted data of fatty acid composition for the catalysts with the highest (Ni/SiG-A) and the lowest (Ni/SiG-B) activity. **Table 12** shows the best fitting kinetic constant values for all three catalysts.

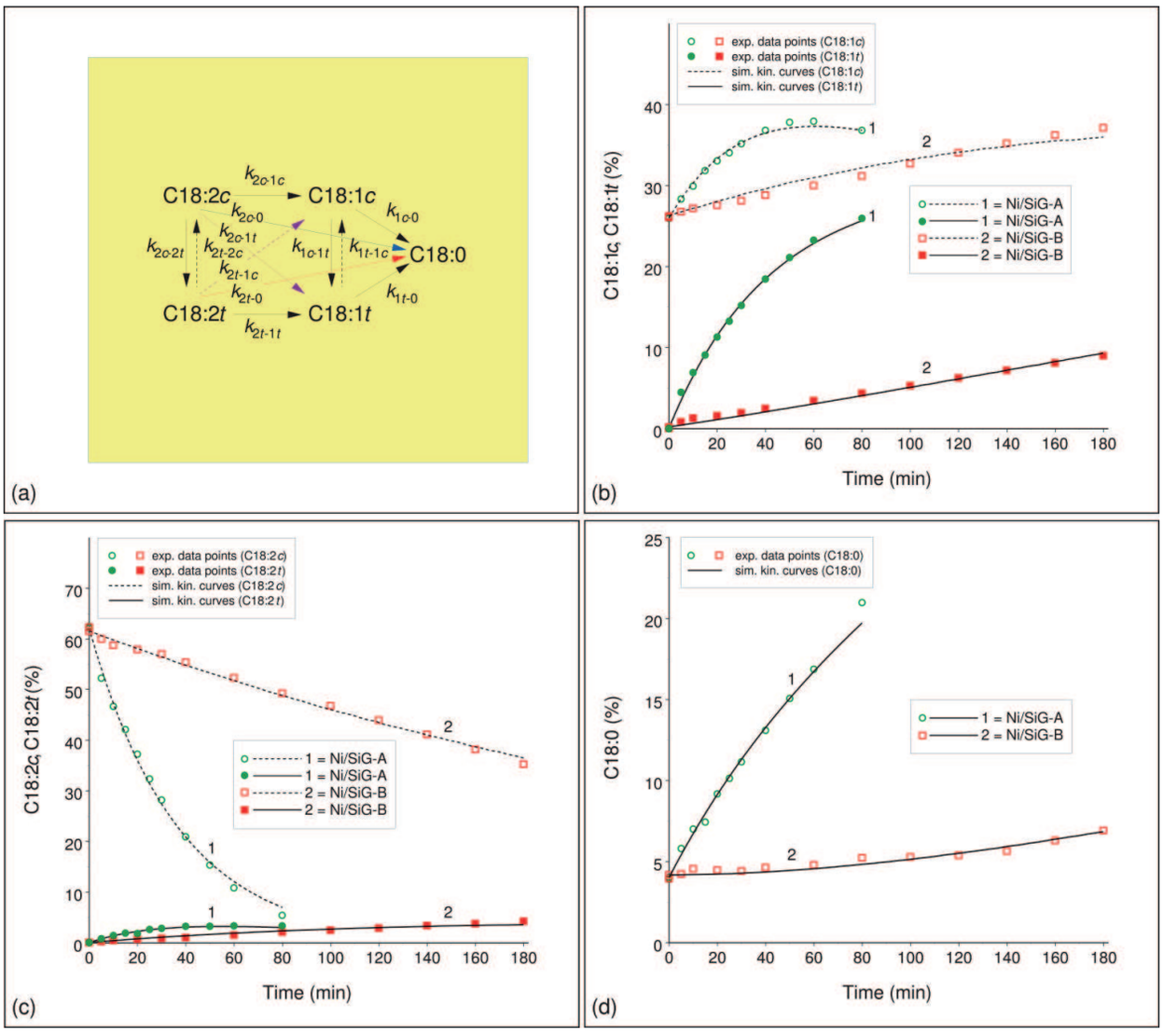

Figure 13. Hydrogenation of SFO: (a) reaction pathway; (b–d) correlation between experimental data and model predictions for SFO hydrogenation over Ni/SiG catalysts under the experimental conditions used.

The results in **Table 12** indicate that the values of the rate constants show a significant difference, regardless of the catalyst activity and hence the contribution of the individual reactions in the reaction mechanism can be recognized.

Rate constants[a]	Sample		
	Ni/SiG-A	Ni/SiG-B	Ni/SiG-C
$k_{2c\text{-}1c}$ (min^{-1})	**9.6×10^{-3}**	**2.3×10^{-3}**	**2.8×10^{-3}**
$k_{2c\text{-}1t}$ (min^{-1})	**1.1×10^{-2}**	1.1×10^{-7}	**2.2×10^{-3}**
$k_{2c\text{-}0}$ (min^{-1})	**4.3×10^{-3}**	8.0×10^{-9}	**2.7×10^{-3}**
$k_{2t\text{-}1t}$ (min^{-1})	8.5×10^{-7}	1.0×10^{-7}	2.4×10^{-7}
$k_{2t\text{-}1c}$ (min^{-1})	2.0×10^{-7}	6.7×10^{-7}	1.4×10^{-6}
$k_{2t\text{-}0}$ (min^{-1})	**1.1×10^{-2}**	**4.7×10^{-3}**	**9.2×10^{-3}**
$k_{2c\text{-}2t}$ (min^{-1})	**2.6×10^{-3}**	**6.3×10^{-4}**	**8.0×10^{-4}**
$k_{2t\text{-}2c}$ (min^{-1})	1.2×10^{-5}	5.3×10^{-7}	2.6×10^{-7}
$k_{1c\text{-}0}$ (min^{-1})	**8.2×10^{-4}**	2.0×10^{-7}	9.2×10^{-8}
$k_{1t\text{-}0}$ (min^{-1})	**1.8×10^{-3}**	**8.7×10^{-4}**	**3.6×10^{-3}**
$k_{1c\text{-}1t}$ (min^{-1})	**2.2×10^{-3}**	**1.7×10^{-3}**	**2.0×10^{-3}**
$k_{1t\text{-}1c}$ (min^{-1})	2.5×10^{-8}	9.3×10^{-10}	4.6×10^{-10}

[a]Values in bold show significant rate constants.

Table 12. Kinetic constant values for Ni/SiG catalysts at 160°C and 0.2 MPa.

In order to simplify the reaction pathway shown in **Figure 13a**, without compromising the accuracy of predicting the concentration of fatty acid change as criteria of importance for some rate constants, we used a value of 1% of the highest rate constant for the particular catalyst (1% k_{max}). Rate constants higher than 1% k_{max} were declared as significant and marked bold in **Table 12**. On the contrary, rate constants less than 1% k_{max} are associated as insignificant. It was shown that the number of significant rate constants increases as the activity of the catalysts grows higher. Significant constants, higher than 1% k_{max}, show that Ni/SiG-A has 8, Ni/SiG-C has 7, while the least active catalyst, Ni/SiG-B, has the lowest value 5. Using the criteria of 1% k_{max}, we can rewrite a reaction pathway (**Figure 13a**), which will include only significant rate constants for each individual catalyst and are given in **Figure 14**.

Using the reduced reaction pathways, reaction rates were rewritten, using only significant rate constants and the process of hydrogenation was simulated with only those reaction rates. Values of rate constants then obtained were the same as the ones obtained by the initial reaction mechanism, which indicates that the reduction of the initial reaction pathway changes as a function of catalyst activity.

http://dx.doi.org/10.5772/66967

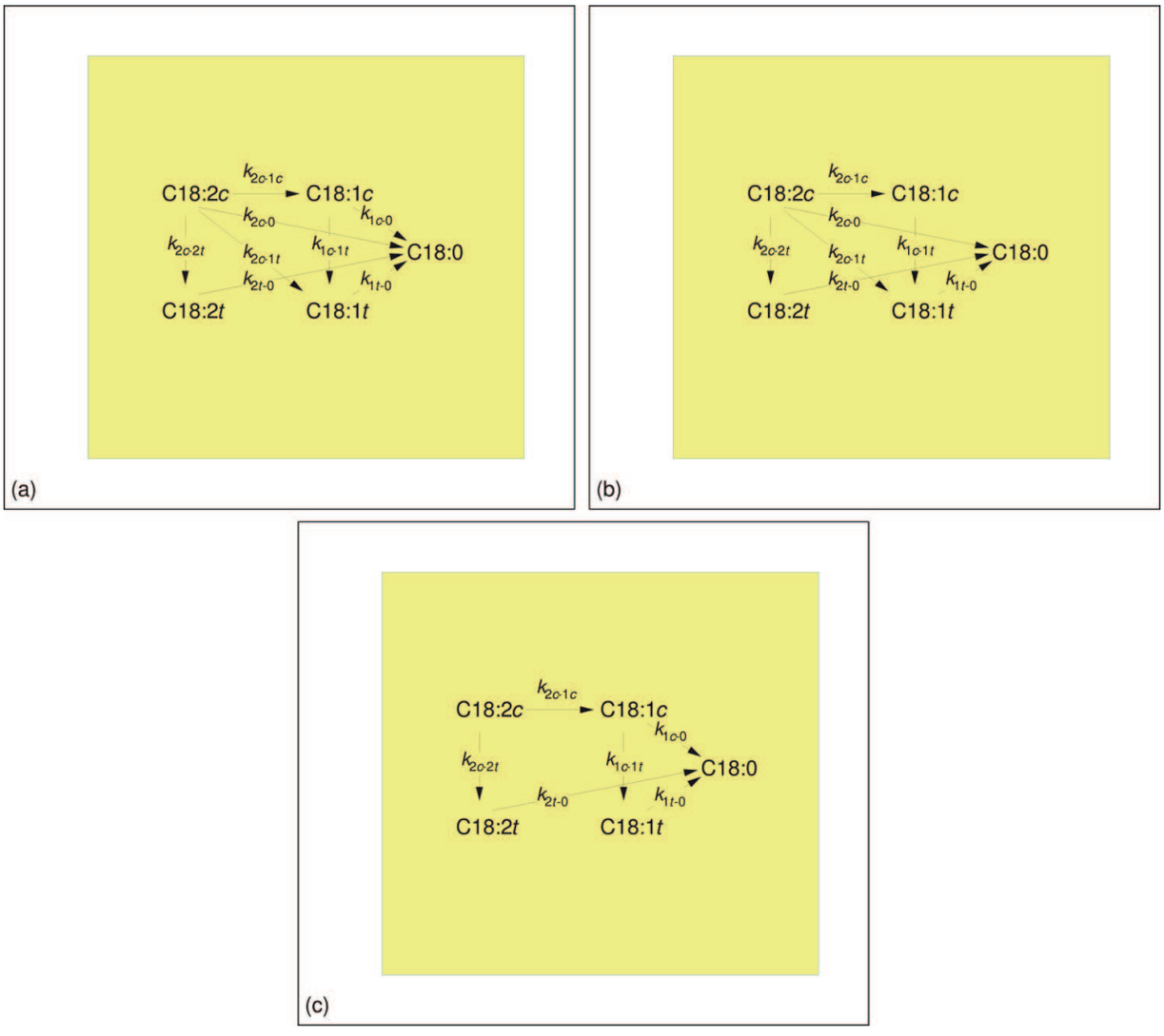

Figure 14. Reduced reaction pathways for three different catalysts: (a) Ni/SiG-A; (b) Ni/SiG-C; (c) Ni/SiG-B.

4. Conclusions

The characteristics, structure and catalytic behavior of high loading nickel-based catalysts supported on diatomite, silica gel and perlite have been analyzed. Nickel-based supported catalyst precursors were prepared by the precipitation-deposition method. The results show that the state, reducibility and dispersion of nickel in supported nickel-based catalysts vary depending on the nature of support and the preparation parameters.

Combined nitrogen physisorption and mercury porosimetry studies showed that the studied nickel-based supported systems had a high specific surface area and a well-developed porous structure, containing mesopores stable to thermal reduction treatments.

The results concerning the influence of the preparation stage and nature of the support and the modifier clearly illustrate the features of the supported Ni^{2+} phase and demonstrate that

IR and XRD measurements may offer as an effective tool to identify nickel species and their interaction with support in differently supported and modified nickel-based catalyst precursors. From the results obtained by both IR and XRD instrumental techniques, it could be concluded that during the deposition reaction under alkaline conditions, the silica as the constitutive component of all studied supports reacts with the basic nickel carbonate precipitate and generates the new supported nickel hydrosilicate phase.

The TPR results demonstrate rather well the differences between Ni compounds formed on the surface of supports. The weak metal-support interaction in the Ni-Mg/PF system is probably responsible for the hydrosilicate formation at a low level, which could decrease the difficulty in the system reduction. The Ni-Mg/D and Ni/SiG systems are difficult to reduce and are comparable in reduction characteristics to nickel hydrosilicates. The addition of silver to the Ni-Mg/D system significantly affected reducibility of nickel-based catalysts. Larger nickel crystallites in silver modified nickel catalysts displayed easier nickel reduction than smaller ones in the Ni-Mg/D catalyst.

The hydrogen chemisorption study showed that the size of nickel nanoparticles obtained in the studied catalyst precursor systems depended on the nature of precursor nickel salt from which they are formed, the kind and loading of metal modifier and the type of support used.

The XPS study of Ni/SiG, Ni-Mg/D and Ni-Mg-Ag/D precursor samples confirm the formation surface species with different strength of interaction and different dispersion of the supported nickel species.

The silver modifier inhibits hydrogenation activity, this effect being more obvious as the Ag loading is higher. Modification by silver allowed us to promote the selectivity toward the *cis* isomers, but the catalyst is less active than the non-modified catalyst in the partial hydrogenation of soybean oil.

Among the catalyst samples studied, the highest activity in the sunflower oil hydrogenation was observed over the Ni-Mg/PF-1 catalyst suggesting that the Ni-Mg/PF-1 catalyst is a promising catalyst for SFO hydrogenation. Although Ni/SiG catalysts show a lower overall activity, this system also could be considered as good, since they produced less amount of stearic acid compared to the Ni-Mg/PF system.

The kinetic models include the saturation of double bonds along the fatty acids chains and *cis*/*trans* isomerization. Under studied operating conditions models proved to adequately fit the experimental data for the evolution of product distribution with reaction time. It was shown that the catalysts of different activities had different reaction pathways. The more active catalysts, the reaction pathways multiply and require more complex reaction scheme to describe the results of the catalytic tests.

Acknowledgments

The authors are grateful to the Ministry of Education, Science and Technological Development of the Republic of Serbia (Project No. III 45001) for providing funding support. The support by Serbian Academy of Sciences and Arts and by Bulgarian Academy of Sciences (Joint Research Project: New nanosized hydrogenation catalysts based on metals of VIII group) is also appreciated.

Author details

Miroslav Stanković[1]*, Jugoslav Krstić[1], Margarita Gabrovska[2], Vojkan Radonjić[1], Dimitrinka Nikolova[2], Davor Lončarević[1] and Dušan Jovanović[1]

*Address all correspondence to: mikastan@nanosys.ihtm.bg.ac.rs

1 Department of Catalysis and Chemical Engineering, Institute of Chemistry, Technology and Metallurgy, University of Belgrade, Belgrade, Serbia

2 Institute of Catalysis, Bulgarian Academy of Sciences, Sofia, Bulgaria

References

[1] Shahidi F, editor. Bailey's Industrial Oil and Fat Products, Volume 4, Edible Oil and Fat Products: Products and Applications. 6th ed. Chichester: Wiley; 2005. 455 p. ISBN: 978-0-471-38549-3

[2] Gunstone FD. Oils and fat in the market place. Commodity oils and fats. Soybean Oil. The AOCS Lipid Library. [Internet]. 2012. Available from: http://lipidlibrary.aocs.org/market/soybean.htm. [Accessed: 2016-05-27]

[3] Hamilton RJ. The chemistry of rancidity in foods. In: Allen JC, Hamilton RJ, editors. Rancidity in Foods. 3rd ed. New York: Chapman and Hall; 1994. p. 1–21.ch1. ISBN: 0-7514-0219-2.

[4] Choe E, Min DB. Mint: Mechanisms and factors for edible oil oxidation. Comprehensive Reviews in Food Science and Food Safety. 2006;**5**:169–186. DOI: 10.1111/j.1541-4337.2006.00009.x

[5] Gunstone FD. Extraction, refining and modification processes. In: Early R, series editor. Oils and Fats in the Food Industry. Chichester: Wiley-Blackwell; 2008. pp. 26–36. DOI: 10.1002/9781444302424.ch3

[6] Chaudhari VR, Ramachandran AP. Mint: Three phase slurry reactors. AIChE Journal. 1980;**26**:177–201. DOI: 10.1002/aic.690260202

[7] Fernández MB, Tonetto GM, Crapiste GH, Damiani DE. Mint: Revisiting the hydrogenation of sunflower oil over a Ni catalyst. Journal of Food Engineering. 2007;**82**:199–208. DOI: 10.1016/j.foodeng.2007.02.010

[8] Ahmad I, Ali A. Mint: Industrial hydrogenation of rapeseed oil with nickel catalyst. Journal of the American Oil Chemists' Society. 1981;**58**:87–88. DOI: 10.1007/BF02672186

[9] Chu YH, Lin LH. Mint: An evaluation of commercial nickel catalysts during hydrogenation of soybean oil. Journal of the American Oil Chemists' Society. 1991;**68**:680–683. DOI: 10.1007/BF02662296

[10] Cizmeci M, Musavi A, Kayahan M, Tekin A. Mint: Monitoring of hydrogenation with various catalyst ratios. Journal of the American Oil Chemists' Society. 2005;**82**:925–929. DOI: 10.1007/s11746-005-1166-3

[11] Babaee Z, Nikoopour H, Safafar H. Mint: A comparison of commercial nickel catalysts effect on hydrogenation of soybean oil. World Applied Sciences Journal. 2007;**2**:621–626. ISSN: 1818-4952. http://www.idosi.org/wasj/wasj2(6)/10.pdf [Accessed: 2016-06-23]

[12] Coenen JWE. Mint: Hydrogenation of edible oils. Journal of the American Oil Chemists' Society. 1976;**53**:382-389. DOI: 10.1007/BF02605727

[13] Balakos MW, Hernandez EE. Mint: Catalyst characteristics and performance in edible oil hydrogenation. Catalysis Today. 1997;**35**:415–425. DOI: 10.1016/S0920-5861(96)00212-X

[14] Sohail A, Chandrappa KG, Bakhtiar M, Jayant I. Mint: Catalytic hydrogenation of soybean oil promoted by synthesized Ni/SiO_2 nanocatalyst. Der Pharma Chemica. 2013;**5**:118–126. http://derpharmachemica.com/vol5-iss2/DPC-2013-5-2-118-126.pdf [Accessed: 2016-06-03]

[15] Stender S, Dyerberg J. Mint: Influence of *trans* fatty acids on health. Annals of Nutrition and Metabolism. 2004;**48**:61–66. DOI: 10.1159/000075591

[16] Tarrago-Trani MT, Phillips KM, Lemar LE, Holden JM. Mint: New and existing oils and fats used in products with reduced *trans*-fatty acid content. Journal of the American Dietetic Association. 2006;**106**:867–880. DOI: 10.1016/j.jada.2006.03.010

[17] Kummerow FA. Mint: The negative effects of hydrogenated *trans* fats and what to do about them. Atherosclerosis. 2009;**205**:458–465. DOI: 10.1016/j.atherosclerosis.2009.03.009

[18] Mensink RP, Katan MB. Mint: Effect of dietary *trans* fatty acids on high-density and low-density lipoprotein cholesterol levels in healthy subjects. The New England Journal of Medicine. 1990;**323**:439–445. DOI: 10.1056/NEJM199008163230703

[19] Wright AJ, Wong A, Diosady LL. Mint: Ni catalysts promotion of a *cis*-selective Pd catalyst for canola oil hydrogenation. Food Research International. 2003;**36**:1069–1072. DOI: 10.1016/j.foodres.2003.08005

[20] Belkacemi K, Boulmerka A, Arul J, Hamoudi S. Mint: Hydrogenation of vegetable oils with minimum *trans* and saturated fatty acid formation over a new generation of Pd-catalyst. Topics in Catalysis. 2006;**37**:113–120. DOI: 10.1007/s11244-006-0012-y

[21] Li T, Zhang W, Lee RZ, Zhong Q. Mint: Nickel-boron alloy catalysts reduce the formation of *trans* fatty acids in hydrogenated soybean oil. Food Chemistry. 2009;**114**:447–452. DOI: 10.1016/j.foodchem.2008.09.068

[22] Stanković M, Gabrovska M, Krstić J, Tzvetkov P, Shopska M, Tsacheva T, Banković P, Edreva-Kardjieva R, Jovanović D. Mint: Effect of silver modification on structure and catalytic performance of Ni-Mg/diatomite catalysts for edible oil hydrogenation. Journal of Molecular Catalysis A: Chemical. 2009;**297**:54–62. DOI: 10.1016/j.molcata.2008.09.004

[23] Hussain ST, Zia F, Mazhar M. Mint: Modified nano supported catalyst for selective catalytic hydrogenation of edible oils. European Food Research and Technology. 2009;**228**:799–806. DOI: 10.1007/s00217-008-0991-y

[24] Alshaibani AM, Yaakob Z, Alsobaai AM, Sahri M. Mint: Palladium-boron catalyst for vegetable oils hydrogenation. RASĀYAN Journal of Chemistry. 2012;**5**:463–467. e-ISSN: 0976-0083

[25] McArdle S, Leahy JJ, Curtin T, Tanner D. Mint: Hydrogenation of sunflower oil over Pt-Ni bimetallic supported catalysts: preparation, characterization and catalytic activity. Applied Catalysis A: General. 2014;**474**:78–86. DOI: 10.1016/j.apcata.2013.08.033

[26] Jang ES, Jung MY, Min DB. Mint: Hydrogenation for *low* trans and high conjugated fatty acids. Comprehensive Reviews in Food Science and Food Safety. 2005;**4**:22–30. DOI: 10.1111/j.1541-4337.2005.tb00069.x

[27] Menaa F, Menaa A, Tréton J, Menaa B. Mint: Technological approaches to minimize industrial *trans* fatty acids in foods. Journal of Food Science. 2013;**78**:377–386. DOI: 10.1111/1750-3841.12055

[28] Mohr C, Claus P. Mint: Hydrogenation properties of supported nanosized gold particles. Since Progress. 2001;**84**:331–334. DOI: 10.3184/003685001783238925

[29] Stanković M, Čupić Ž, Gabrovska M, Banković P, Nikolova D, Jovanović D. Mint: Characteristics and catalytic behaviour of supported NiMgAg/D catalysts in the partial hydrogenation of soybean oil. Reaction Kinetics, Mechanisms and Catalysis. 2015;**115**:105–127. DOI: 10.1007/s11144-014-0829-5

[30] Krstić J, Gabrovska M, Lončarević D, Nikolova D, Radonjić V, Vukelić N, Jovanović D. Mint: Influence of Ni/SiO_2 activity on the reaction pathway in sunflower oil hydrogenation. Chemical Engineering Research and Design. 2015;**100**:72-80. DOI: 10.1016/j.cherd.2015.05.001

[31] Radonjić V, Krstić J, Lončarević D, Jovanović D, Vukelić N, Stanković M, Nikolova D, Gabrovska M. Mint: Perlite as a potential support for nickel catalyst in the process of sunflower oil hydrogenation. Russian Journal of Physical Chemistry A. 2015;**89**:2359–2366. DOI: 10.1134/S0036024415130294

[32] Nohair B, Especel C, Marécot P, Montassier C, Hoang LC, Barbier J, Mint: Selective hydrogenation of sunflower oil over supported precious metals. Comptes Rendus Chimie. 2004;**7**:113–118. DOI: 10.1016/j.crci.2003.10.012

[33] Simakova IL, Simakova OA, Romanenko AV, Murzin DYu. Mint: Hydrogenation of vegetable oils over Pd on nanocomposite carbon catalysts. Industrial and Engineering Chemistry Research. 2008;**47**:7219–7225. DOI: 10.1021/ie800663j

[34] Iida H, Itoh D, Minowa S, Yanagisawa A, Igarashi A: Hydrogenation of soybean oil over various platinum catalysts: effect of support materials on *trans* fatty acid levels. Catalysis Communications. 2015;**62**:1–5. DOI: 10.1016/j.catcom.2014.12.025

[35] Babu GP, Ghuge KD, Rammohan SV, Krishnan V, Bhat AN. Mint: Characterization of silica supported Ni and Mg basic carbonate catalysts precursors. Catalysis Letters. 1992;**15**:95–103. DOI: 10.1007/BF00770902

[36] Thunyaratchatanon C, Jitjamnong J, Luengnaruemitchai A, Numwong N, Chollacoop N, Yoshimura Y. Mint: Influence of Mg modifier on *cis-trans* selectivity in partial hydrogenation of biodiesel using different metal types. Applied Catalysis A: General. 2016;**520**:170–177. DOI: 10.1016/j.apcata.2016.04.019

[37] Parry JD, Winterbottom JM. Mint: The hydrogenation of triglycerides using supported alloy catalysts. I. Silica-supported Ni-Ag catalysts. Journal of Chemical Technology and Biotechnology. 1991;**50**:67–80. DOI: 10.1002/jctb.280500108

[38] Parry JD, Winterbottom JM. Mint: The hydrogenation of triglycerides using supported alloy catalysts. II. Silica-supported Pd-Cu catalysts. Journal of Chemical Technology and Biotechnology. 1991;**50**:81–90. DOI: 10.1002/jctb.280500109

[39] Ksibi Z, Ghorbel A, Bellamy B, Masson A. Mint: Size particle effect and copper or silver addition effect on catalytic properties of rhodium supported onto amorphous silica. Studies in Surface Science and Catalysis. 2000;**130**:2045–2050. DOI: 10.1016/S0167-2991(00)80769-7

[40] Fernández MB, Piqueras CM, Tonetto GM, Crapiste G, Damiani DE. Mint: Partial hydrogenation of sunflower oil: use of edible modifiers of the *cis*/*trans*-selectivity. Journal of Molecular Catalysis A: Chemical. 2005;**233**:133–139. DOI: 10.1016/j.molcata.2005.02.012

[41] Nitta Y, Imanaka T, Teranishi S. Mint: Preparation chemistry of precipitated Ni-SiO_2 catalysts for enantioselective hydrogenation. Journal of Catalysis. 1985;**96**:429–438. DOI: 10.1016/0021-9517(85)90312-4

[42] Nele M, Vidal A, Bhering DL, Pinto JC, Salim VMM. Mint: Preparation of high loading silica supported nickel catalysts: simultaneous analysis of the precipitation and aging steps. Applied Catalysis A: General. 1999;178:177–189. DOI: 10.1016/S0926-860X(98)00285-3

[43] Bhering DL, Nele M, Pinto JC, Salim VMM. Mint: Preparation of high loading silica supported nickel catalysts: analysis of the reduction step. Applied Catalysis A: General. 2002;**234**:55–64. DOI: 10.1016/S0926-860X(02)00198-9

[44] Song CJ, Park TJ, Moon SH. Mint: Properties of the Ni/kieselguhr catalysts prepared by precipitation method. Korean Journal of Chemical Engineering. 1985;**9**:159–163. DOI: 10.1007/BF02705133

[45] Poncelet G, Grange P, Jacobs PA editors. Volume 16. Preparation of Catalysts III. 1st ed. Scientific Bases for the Preparation of Heterogeneous Catalysts. Amsterdam: Elsevier; 1983. 852 p. Electronic ISBN: 9780080960517. Print ISBN: 978044421845.

[46] Burattin P, Che M, Louis C. Mint: Molecular approach to the mechanism of deposition-precipitation of the Ni(II) phase on silica. The Journal of Physical Chemistry B. 1998;**102**:2722–2732. DOI: 10.1021/jp980018k

[47] Coenen JWE. Mint: Characterization of the standard nickel/silica catalyst EuroNi-1 II. Chemical aspects: precipitation, reduction and chemical analysis. Applied Catalysis. 1989;**54**:65–78. DOI: 10.1016/S0166-9834(00)82355-6

[48] van Voorthuijsen van Eijk JJB, Franzen P. Mint: Structure and properties of compounds formed during the preparation of nickel-on-silica catalysts. Recueil des Travaux Chimiques des Pays-Bas. 1951;**70**: 793–812. DOI: 10.1002/recl.19510700906

[49] Montes M, Penneman de Bosscheyde Ch, Hodnett BK, Delannay, Grange P, Delmon B. Mint: Influence of metal-support interactions on the dispersion, distribution, reducibility and catalytic activity of Ni/SiO_2 catalysts. Applied Catalysis. 1984;**12**:309–330. DOI: 10.1016/S0166-9834(00)81670-X

[50] El-Shatorry Y, deMan L, deMan JM. Mint: Evaluation of hydrogenation catalyst activity. Journal of the American Oil Chemists' Society. 1980;**57**:402–404. DOI: 10.1007/BF02678924

[51] Dafler JR. Mint: Nickel crystallite size and net activity of hydrogenation catalysts. Journal of the American Oil Chemists' Society. 1977;**54**:17–23. DOI: 10.1007/BF02671367

[52] Gray JI, Russel LF. Mint: Hydrogenation catalysts—Their effect on selectivity. Journal of the American Oil Chemists' Society. 1979;**56**:36–44. DOI: 10.1007/BF02671758

[53] Martin GA, Mirodatos C, Praliaud H. Mint: Chemistry of silica-supported catalyst: preparation, activation and reduction. Applied Catalysis. 1981;**1**:367–382. DOI: 10.1016/0166-9834(81)80054-1

[54] Ghuge KD, Bhat AN, Babu GP. Mint: Identification of nickel species and their interaction with the support in Ni-silica catalyst precursor. Applied Catalysis A: General. 1993;**103**:183–204. DOI: 10.1016/0926-860X(93)85051-P

[55] Pilar Gonzáles-Marcos M, Gutiérrez-Ortiz José I, Gonzáles-Ortiz de Elguea C, Delgado José A, Gonzáles-Velasko Juan R. Mint: Nickel on silica systems. Surface features and their relationship with support, preparation procedure and nickel content. Applied Catalysis A: General. 1997;**162**:269–280. DOI: 10.1016/S0926-860X(97)00111-7

[56] Burattin P, Che M, Louis C. Mint: Metal particle size in Ni/SiO_2 prepared by deposition-precipitation: influence of the nature of the Ni(II) phase and of its interaction with the support. The Journal of Physical Chemistry B. 1999;**103**:6171–6178. DOI: 10.1021/jp990115t

[57] Gabrovska M, Krstić J, Tzvetkov P, Tenchev K, Shopska M, Vukelić N, Jovanović D. Mint: Effect of the support and the reduction temperature on the formation of metallic nickel phase in Ni/silica gel precursors of vegetable oil hydrogenation catalysts. Russian Journal of Physical Chemistry A. 2011;**85**:2392–2398. DOI: 10.1134/S0036024411130073

[58] Horiuti I, Polanyi M. Mint: Exchange reactions of hydrogen on metallic catalysts. Transactions of the Faraday Society. 1934;**30**:1164–1172. DOI: 10.1039/TF9343001164

[59] Albright LF, Wisniak J. Mint: Selectivity and isomerization during partial hydrogenation of cottonseed oil and methyl oleate: Effect of operating variables. Journal of the American Oil Chemists' Society. 1962;**39**:14–19. DOI: 10.1007/BF02633340

[60] Litchfield C, Lord JE, Isbell AF, Reiser R. Mint: *Cis-trans* isomerization of oleic, linoleic and linolenic acids. Journal of the American Oil Chemists' Society. 1963;**40**:553–557. DOI: 10.1007/BF02822465

[61] Gut G, Kosinka J, Prabucki A, Schuerch A. Mint: Kinetics of the liquid-phase hydrogenation and isomerization of sunflower seed oil with nickel catalysts. Chemical Engineering Science. 1979;**34**:1051–1056. DOI: 10.1016/0009-2509(79)80005-6

[62] Ray JD, Carr BT. Mint: Empirical modeling of soybean oil hydrogenation. Journal of the American Oil Chemists' Society. 1985;**62**:1218–1222. DOI: 10.1007/BF02541831

[63] Niklasson C andersson B, Schöön NH. Mint: Influence of hydrogen pressure on selectivity in consecutive hydrogenation reactions. Industrial and Engineering Chemistry Research. 1987;**26**:1459–1463. DOI: 10.1021/ie00067a031

[64] Grau RJ, Cassano AE, Baltanás MA. Mint: Catalysts and network modeling in vegetable oil hydrogenation processes. Catalysis Reviews Science and Engineering. 1988;**30**:1–48. DOI: 10.1080/01614948808078615

[65] Machado RM, Gaumer Freidl K, Achenbach ML. Impact of catalysts on selectivity and reaction rates for the hydrogenation of soybean oil. In: 9th RC User Forum Europe, October 1999; Berne: EU99_11; 1999. pp. 1–12

[66] Santana A, Larrayoz MA, Ramírez E, Nistal J, Recasens F. Mint: Sunflower oil hydrogenation on Pd in supercritical solvents: kinetics and selectivities. The Journal of Supercritical Fluids. 2007;**41**:391–403. DOI: 10.1016/j.supflu.2006.12.009

[67] Jovanovic D, Radovic R, Mares Lj, Stankovic M, Markovic B. Mint: Nickel hydrogenation catalyst for tallow hydrogenation and for the selective hydrogenation of sunflower seed oil and soybean oil. Catalysis Today. 1998;**43**:21–28. DOI: 10.1016/S0920-5861(98)00133-3

[68] Nikolova D, Krstić J, Spasov L, Simeonov D, Lončarević D, Stefanov Pl, Jovanović D. Mint: Surface properties of the Ni-silica gel catalyst precursors for the vegetable oil hydrogenation process: N_2 sorption and XPS studies. Russian Journal of Physical Chemistry A. 2011;**85**:2380–2385. DOI: 10.1134/S0036024411130188

[69] Stanković M, Radonjić V, Krstić J, Marinković D. Preparation of Ni/diatomite hydrogenation catalyst precursors: Effect of counter ions on textural characteristics. In: Proceedings of 12th International Conference on Fundamental and Applied Aspects of Physical Chemistry (Physical Chemistry 2014); 22–26 September 2014; Belgrade: SPCS; 2014. pp. 284–287.

[70] Diefenbacker A, Pocklington WD, editors. Standard Methods for the Analysis of Oils, Fats and Derivatives. 7th ed. 1st Supplement Section 2, 2.001. IUPAC. Oxford: Alden Press; 1992. 151 p. ISBN 0-632-03337-I. [internet]. 2012 Available from: http://old.iupac.org/publications/books/ISBN0632033371_compress.pdf. [Accessed: 2016-06-03]

[71] Coenen JWE, Linsen BG. Structure and activity of silica-supported nickel catalysts. In Linsen BG, Fortuin JMH, Okkerse C, Steggerda JJ editors. Physical and Chemical Aspects of Adsorbents and Catalysts. London and New York: Academic Press; 1970. Ch. 10. pp. 471–527.

[72] Echeverria SM andres VM. Mint: Effect of the method of preparation on the activity of nickel-kieselguhr catalyst for vegetable oil hydrogenation. Applied Catalysis. 1990;**66**:73–90. DOI: 10.1016/S0166-9834(00)81628-0

[73] Burattin P, Che M, Louis C. Mint: Characterization of the Ni(II) phase formed on silica upon deposition-precipitation. The Journal of Physical Chemistry B. 1997;**101**:7060–7074. DOI: 10.1021/jp970194d

[74] Kermarec M, Carriat JY, Burattin P, Che M, Decarreau A. Mint: FTIR identification of the supported phases produced in the preparation of silica-supported nickel catalysts. The Journal of Physical Chemistry. 1994;**98**:12008–12017. DOI: 10.1021/j100097a029

[75] Ikuhara YH, Saito T, Takahashi S, Sasaki Y, Hirayama T. Mint: Synthesis and microstructural analysis of homogeneously dispersed nickel nanoparticles in amorphous silica. Journal of the American Ceramic Society. 2012;**95**:524–529. DOI: 10.1111/j.1551-2916.2011.04897.x

[76] Sodeyama K, Sakka Y, Kamino. Mint: Preparation of fine expanded perlite. Journal of Materials Science. 1999;**34**:2461–2468. DOI: 10.1023/A:1004579120164

[77] Sohn JR. Mint: Catalytic activities of nickel-containing catalysts for ethylene dimerization and butane isomerization and their relationship to acidic properties. Catalysis Today. 2002;**73**:197–209. DOI: 10.1016/S0920-5861(01)00513-2

[78] van Dillen AJ, Geus JW, Hermans LAM, van der Meijden J. Production of supported copper and nickel catalysts by deposition-precipitation. In: Proceedings of the Sixth International Congress on Catalysis, Imperial College; 12–16 July 1976; London. Letchworth, England: Chemical Society; 1977. pp. 667–685.

[79] Geus JW. Mint: Production and thermal pre-treatment of supported catalysts. Studies in Surface Science and Catalysis. Elsevier Science. eBook 1983;**16**:1–33. ISBN: 9780080960517, Print ISBN: 9780444421845.

[80] Houalla M. Mint: An assessment of the influence of the preparation method, the nature of the carrier and the use of additives on the state, dispersion and reducibility of a deposited "nickel oxide" phase. Studies in Surface Science and Catalysis. Elsevier Science. eBook 1983;**16**:273–289. ISBN: 9780080960517, Print ISBN: 9780444421845.

[81] Anderson JA, Rodrigo MT, Daza L, Mendioroz S. Mint: Influence of the support in the selectivity of nickel/clay catalysts for vegetable oil hydrogenation. Langmuir. 1993;**9**:2485–2490. DOI: 10.1021/la00034a001

[82] Kibby CL, Massoth FE, Swift HE. Mint: Surface properties of hydrogen-reduced nickel chrysotiles. Journal of Catalysis. 1976;**42**:350–359. DOI: 10.1016/0021-9517(76)90109-3

[83] Jacobs PA, Nijs HH, Poncelet G. Mint: Characterization of reduced natural garnierite and its catalytic activity for carbon monoxide hydrogenation. Journal of Catalysis. 1980;**64**:251–259. DOI: 10.1016/0021-9517(80)90500-X

[84] Gabrovska M, D. Nikolova, Krstić J, Stanković M, Stefanov P, Edreva-Kardjieva, Jovanović D. Mint: The state of nickel in the silver modified NiMg/SiO_2 vegetable oil hydrogenation catalysts. Russian Journal of Physical Chemistry A. 2009;**83**:1461–1467. DOI: 10.1134/S0036024409090088

[85] Wang W. High nickel- and titania-containing mesoporous silicas: synthesis and characterisation [doctoral thesis]. Leicestershire, UK: Loughborough University, Institute of Polymer Technology and Materials Engineering; 2005.

[86] Turlier P, Praliaud H, Moral P, Martin GA, Dalmon JA. Mint: Influence of the nature of the support on the reducibility and catalytic properties of nickel: evidence for a new type of metal support interaction. Applied Catalysis. 1985;**19**:287–300. DOI: 10.1016/S0166-9834(00)81751-0

[87] Roman A, Delmon B. Mint: Promoter and carrier effects in the reduction of NiO/SiO_2. Journal of Catalysis. 1973;**30**:333–342. DOI: 10.1016/0021-9517(73)90148-6

[88] Richardson JT, Turk B, Lei M, Forster K, Twigg MV. Mint: Effects of promoter oxides on the reduction of nickel oxide. Applied Catalysis A: General. 1992;**83**:87–101. DOI: 10.1016/0926-860X(92)80028-B

[89] Coenen JWE. Mint: Reduction of silica supported nickel catalysts. Studies in Surface Science and Catalysis. Elsevier Science. 1979;**3**:89–108. ISBN: 0-444-41733-8 (Vol 3), ISBN: 0-444-41801-6 (Series).

[90] Gabrovska M, Krstić J, Edreva-Kardjieva R, Stanković M, Jovanović D. Mint: The influence of the support on the properties of nickel catalysts for edible oil hydrogenation. Applied Catalysis A: General. 2006;**299**:73–83. DOI: 10.1016/j.apcata.2005.10.011

[91] Boudjahem A-G, Monteverdi S, Mercy M, Ghanbaja D, Bettahar MM. Mint: Nickel nanoparticles supported on silica of low surface area. Hydrogen chemisorption and TPD catalytic properties. Catalysis Letters. 2002;**84**:115–122. DOI: 10.1023/A:1021093005287

[92] Mustard DG, Bartholomew CH. Mint: Determination of metal crystallite size and morphology in supported nickel catalysts. Journal of Catalysis. 1981;**67**:186–206. DOI: 10.1016/0021-9517(81)90271-2

[93] Bartholomew CH. Mint: Hydrogen adsorption on supported cobalt, iron and nickel. Catalysis Letters. 1990;**7**:27–51. DOI: 10.1007/BF00764490

[94] Kumar N, King TS, Vigil RD. Mint: A portal model for structure sensitive hydrogen adsorption on $Ru\text{-}Ag/SiO_2$ catalysts. Chemical Engineering Science. 2000;**55**:4973–4979. DOI: 10.1016/S0009-2509(00)00132-9

[95] Gubitosa G, Berton A, Camia M, Pernicone N. Mint: Influence of the preparation technique of Pd-silica catalysts on metal dispersion and catalytic activity. Studies in Surface Science and Catalysis. Elsevier Science. eBook 1983;**16**:431–438. ISBN: 9780080960517, Print ISBN: 9780444421845.

[96] Wu M, Hercules DM. Mint: Studies of supported nickel catalysts by X-ray photoelectron and ion scattering spectroscopies. The Journal of Physical Chemistry. 1979;**83**:2003–2008. DOI: 10.1021/j100478a015

[97] Shalvoy RB, Reucroft PJ, Davis BH. Mint: Characterization of coprecipitated nickel on silica methanation catalysts by X-ray photoelectron spectroscopy. Journal of Catalysis. 1979;**56**:336–348. DOI: 10.1016/0021-9517(79)90126-X

[98] Rodrigo MT, Daza L, Mendioroz S. Mint: Nickel supported on natural silicates: Activity and selectivity in sunflower seed oil hydrogenation. Applied Catalysis A: General. 1992;**88**:101–114. DOI: 10.1016/0926-860X(92)80198-L

[99] Briggs D. Handbook of X-ray Photoelectron Spectroscopy. Eden Prairie, Minnesota: Perkin Elmer Corp., Physical Electronics Division; 1979. 190 p. DOI: 10.1002/sia.740030412

[100] Venezia AM. Mint: X-ray photoelectron spectroscopy (XPS) for catalysts characterization. Catalysis Today. 2003;**77**:359–370. DOI: 10.1016/S0920-5861(02)00380-2

[101] Gaarenstroom SW, Winograd N. Mint: Initial and final state effects in the ESCA spectra of cadmium and silver oxides. The Journal of Chemical Physics. 1977;**67**:3500–3506. DOI: 10.1063/1.435347

[102] Lefèbvre VJ, Baltes J. Mint: Nickel/Silber-hydrierkatalysatoren und ihre verwendung zur selektiven härtung von fetten. European Journal of Lipid Science and Technology. First published: Fette, Seifen, Ansitrichmittel. 1975;**77**:125–131. DOI: 10.1002/lipi.19750770402. [Internet]. 2006. Available from: http://onlinelibrary.wiley.com/doi/10.1002/lipi.v77:4/issuetoc [Accessed: 2016-06-08]

[103] Macher M. Supercritical hydrogenation of vegetable oils [PhD thesis]. Göteborg: Chalmer University of Technology; 2001.

[104] Albright LF, Allen RR, Moore MC. Mint: Quantitative measure of geometrical isomerization during the partial hydrogenation of triglyceride oils. Journal of the American Oil Chemists' Society. 1970;**47**:295–298. DOI: 10.1007/BF02609498

[105] Chen AH, McIntire DD, Allen RR. Mint: Modeling of reaction rate constants and selectivities in soybean oil hydrogenation. Journal of the American Oil Chemists' Society. 1981;**58**:816–818. DOI: 10.1007/BF02665587

[106] Jovanović D, Čupić Ž, Stanković M, Rožić Lj, Marković B. Mint: The influence of the isomerization reactions on the soybean oil hydrogenation process. Journal of Molecular Catalysis A: Chemical. 2000;**159**:353–357. DOI: 10.1016/S1381-1169(00)00154-0

[107] Belkacemi K, Boulmerka A, Hamoudi S, Arul J. Mint: Activity and selectivity of novel structured Pd catalysts: kinetics modelling of vegetable oils hydrogenation. International Journal of Chemical Reactor Engineering. 2005;**3**:A59. 1–25. ISSN: 2194-5748. http://www.bepress.com/ijcre/vol3/A59 [Accessed: 2016-07-18]

[108] Gear CW. Numerical initial value problems in ordinary differential equations. Englewood Cliffs, New Jersey: Prentice-Hall; 1971. 253 p.

[109] Stone RE, Tovey CA. Mint: The simplex and projective scaling algorithms as iteratively reweighted least squares methods. SIAM Review. 1991;**33**:220–237. DOI: 10.1137/1033049

[110] Pilar Gonzáles-Marcos M, Gutiérrez-Ortiz José I, Gonzáles-Ortiz de Elguea C, Alvarez Jon I, Gonzáles-Velasko Juan R. Mint: Control of the product distribution in the hydrogenation of vegetable oils over nickel on silica catalysts. The Canadian Journal of Chemical Engineering. 1998;**76**:927–935. DOI: 10.1002/cjce.5450760510

IntechOpen